

Master's Degree Thesis in the Course of Environmental and Land Engineering

# Microalgae Lysis through Hydrodynamic Cavitation

Supervisor:	Candidate:	

Prof. Costantino Manes

Samira Naghashzargar

**Co-Supervisor:** 

Prof. Vincenzo Andrea Riggio

October 2025

## **Table of Contents**

List	of Fig	ures		V
List	of Tal	oles		viii
Ack	mowle	dgement	ts	ix
Abs	stract			x
1	Intro 1.1		round	
	1.2	Proble	m statement	2
	1.3	Thesis	objectives	2
2	Liter 2.1		eviewalgae Structure and Lysis Techniques	
	2.2	Cavita	tion Phenomenon	6
		2.2.1	Thermodynamic trigger: Vapor Pressure	7
		2.2.2	Hydrodynamic origin of low pressure	8
		2.2.3	Definition and Types of Nucleation	9
		2.2.4	Bubble Dynamics	10
	2.3	Hydro	dynamic Cavitation (HC)	11
		2.3.1	Cavitation Number	11
	2.4	Reacto	or Designs for Hydrodynamic Cavitation	13
		2.4.1	Head Loss in Orifice Plates	15
	2.5	Cavita	tion Intensity Requirements for Microalgae Cell W	all Rupture
		17		
3	Mate	aterials and Methodsl  Experimental Facility Description		
		3.1.1	Hydraulic Circuit	20
		3.1.2	High-speed camera	22
	3.2	Evalua	ation of Methods to Lower Cavitation Number	23
		3.2.1	Pump Configuration	24

		3.2.2	Orifice Plates	25
	3.3	Analyt	ical Methods and Data Collection	26
	3.4	Prelim	inary Manual Cavitation Test in Sealed Glass Chamber	29
	3.5	Algae	Preparation for Hydrodynamic Cavitation	30
4	Resu		Discussionsdynamic Characterization	
		4.1.1	Head Loss Coefficient	33
		4.1.2	Comparison of Measurements with Empirical Laws	37
	4.2	Microa	algae-Lysis Assessment under Cavitating Flow	46
5 Co	onclusi	on and F	Recommendations	49
Refe	erences	S		51
App	endix.			56

## **List of Figures**

Figure 1 Different cell disruption techniques for microalgae(Rahman et al.,
2022)
Figure 2 Mechanism of hydrodynamic cavitation (1) Generation of nuclei, (2)
Expansion of bubbles to maximum, (3) Collapse of bubble, (4) Bang-
release of energy.(Waghmare et al., 2019)
Figure 3 Phase Diagram(Franc & Michel, 2005)
Figure 4 Schematic of pressure distribution on a streamline(Brennen, 2013)13
Figure 5 Illustration of a different orifice design. DO: diameter of orifice; DP:
diameter(Zheng et al., 2022)14
Figure 6 Orifice plate hydrodynamic cavitation setup.(Gogate & Kabadi, 2009).15
Figure 7 (a) Experimental hydraulic circuit setup. (b) Schematic of the hydraulic
circuit21
Figure 8 Transparent cavitation chamber
Figure 9 High-speed camera setup (Photron FASTCAM Nova S16) used for
Figure 9 High-speed camera setup (Photron FASTCAM Nova S16) used for cavitation bubble observation.
cavitation bubble observation

Figure	14 Variation of head-loss coefficient k with Reynolds number for the four
	tested orifice diameters (2 mm, 3 mm, 4.5 mm, 6 mm)35
Figure	15 Head-loss coefficient k as a function of cavitation number $Cv$ for the
	four orifice diameters
Figure	16 High-speed imaging snapshots showing cavitation bubble formation for
	four different orifice diameters: (a) 2 mm,(b) 3 mm,(c) 4.5 mm,(d) 6 mm.
	The images highlight differences in vapor bubble size and distribution
	under similar flow conditions
Figure	17 Comparison between experimental and empirical discharge coefficients
	for the 2 mm orifice:(a) variation of Cd with Reynolds number;(b)
	variation of <i>Cd</i> with cavitation number41
Figure	18 Comparison between experimental and empirical discharge coefficients
	for the 3 mm orifice:(a) variation of <i>Cd</i> with Reynolds number;(b)
	variation of <i>Cd</i> with cavitation number42
Figure	19 Comparison between experimental and empirical discharge coefficients
	for the 4.5 mm orifice:(a) variation of <i>Cd</i> with Reynolds number;(b)
	variation of <i>Cd</i> with cavitation number43
Figure	20 Comparison between experimental and empirical discharge coefficients
	for the 6 mm orifice:(a) variation of Cd with Reynolds number;(b)
	variation of <i>Cd</i> with cavitation number44
Figure 2	21 Discharge-coefficient trends for round- and sharp-edged orifices as a
	function of injection pressure differential $\Delta P$ , illustrating cavitation onset
	and the subsequent "hydraulic-flip" plateau; (a) $d = 0.5$ mm and (b) $d = 1$
	mm. Source: Chemloul et al., 201246
Figure 2	22 Bright-field micrograph of Galdieria sulphuraria suspension before
	cavitation treatment (40× magnification)

Figure	23 Bright-field microscopic images of Galdieria sulphuraria after 10, 20,	
	30, and 50 flow turnovers through the hydrodynamic cavitation system	
	(40× magnification)	48
Figure	24 Appendix A .Suggested Venturi Design with Flange Connections –	
	Dimensional and Assembly Drawings	56

## **List of Tables**

Table	l Treatment duration	and sample c	oncentration f	for different tui	rnover cycles
	of algae suspension	in the hydrod	ynamic cavita	ation experimen	nt31

## Acknowledgements

I want to sincerely thank Professor Costantino Manes for his patience, kindness, and steady guidance throughout this work. His support helped me move forward in every stage of this journey. I'm also grateful to Dr. Bosio and the lab assistants for their valuable help, and to Professor Vincenzo Andrea Riggio for his support.

To my family, who were far from me but somehow always close—I don't know how you do it, but your belief in me never seemed to fade, even when mine did.

And to my beloved Loobia, simply because being there was enough. You were with me in silence, and that mattered more than anything.

### **Abstract**

Hydrodynamic cavitation occurs when vapor bubbles form and subsequently collapse due to localized pressure drops in a flowing fluid. This phenomenon holds significant potential for applications such as microalgae cell disruption, as the collapse of bubbles releases high-energy shockwaves capable of rupturing robust cell walls. The primary objective of this thesis was to investigate whether hydrodynamic cavitation could be effectively exploited for lysing *Galdieria sulphuraria* microalgae.

The research focused on the hydrodynamic characterization necessary to optimize microalgae cell disruption. Experiments were conducted using a custom-designed stainless-steel hydraulic circuit, incorporating interchangeable orifice plates with diameters of 2 mm, 3 mm, 4.5 mm, and 6 mm. Systematic characterization involved measuring upstream and downstream pressures, flow rates, and utilizing high-speed imaging techniques to qualitatively evaluate bubble dynamics. This comprehensive approach enabled the analysis of how changes in orifice dimensions influenced cavitation number and bubble characteristics, which directly impact the effectiveness of microalgae cell disruption.

Initial manual cavitation tests were conducted using a sealed glass container to visually observe bubble formation and collapse across varying algae-water mixtures. High-speed imaging was employed throughout to perform qualitative analyses of bubble sizes and cavitation intensities under different experimental conditions.

Experimental findings revealed that the 2 mm orifice diameter generated lower cavitation numbers due to higher fluid velocities and greater pressure differentials. Despite these intensified cavitation conditions, the resulting vapor bubbles were smaller, providing insufficient energy upon collapse to effectively disrupt microalgae cells. Conversely, larger orifice diameters produced significantly larger vapor bubbles with greater collapse energy. However, these larger orifices were

unable to achieve sufficiently low cavitation numbers due to limited fluid velocities. Thus, no effective cell disruption occurred at the smallest orifice diameter of 2 mm despite its intense cavitation regime.

Based on these results, it is concluded that further advancements are necessary in reactor design to simultaneously achieve low cavitation numbers and large bubble implosions. Accordingly, an improved cavitation reactor configuration, coupled with a newly proposed pumping system designed to achieve higher cavitation intensities, is suggested for future work.

## 1 Introduction

## 1.1 Background

Microalgae serve as an excellent renewable biomass resource due to their rapid growth rates, minimal land use, and ability to produce diverse valuable bioproducts, including biofuels, proteins, lipids, and nutraceutical compounds. They are increasingly recognized for their potential in sustainable food and feed production, wastewater treatment, carbon sequestration, and energy applications(Aarthy et al., 2018). The complete utilization of microalgae faces major obstacles because of inefficient and expensive cell disruption methods, which represent a vital step in algae biomass processing. Effective lysis methods are essential for breaking down resilient microalgal cell walls, enabling the extraction and recovery of intracellular bioactive compounds. Traditional cell disruption methods, including mechanical techniques (bead milling, high-pressure homogenization), chemical treatments, and enzymatic lysis, often require substantial energy inputs, operational costs, and the use of environmentally harmful solvents(Sousa et al., 2023). Consequently, there is a growing emphasis on exploring innovative technologies capable of overcoming these drawbacks.

Among emerging alternatives, hydrodynamic cavitation has gained considerable attention due to its promising effectiveness and environmental sustainability. Hydrodynamic cavitation leverages fluid mechanical principles to induce localized bubble formation and collapse, generating intense shear forces and localized high temperatures. This mechanism has shown significant potential for efficiently rupturing microalgal cell walls, enhancing the extraction of intracellular compounds without relying on hazardous chemicals or excessive energy consumption(Arya et al., 2023). Hydrodynamic cavitation (HC) has been reported as highly energy-efficient for cell disruption, though performance remains species-dependent and effectiveness varies with cell-wall structure (Lee et al., 2015). Given the growing demand for sustainable, cost-effective algae processing technologies,

advancing the understanding and optimization of hydrodynamic cavitation for microalgal lysis represents an important area of research and innovation.

### 1.2 Problem statement

Hydrodynamic cavitation shows strong promise for algae cell disruption; however, several technical and operational challenges remain. One critical issue is accurately controlling cavitation intensity, as insufficient cavitation leads to incomplete cell disruption, while excessively intense cavitation may degrade valuable intracellular compounds due to extreme shear forces and heat generation. Furthermore, the efficiency of hydrodynamic cavitation depends heavily on three main factors, which include chamber design, fluid characteristics, and operating parameters (Kim et al., 2015).

## 1.3 Thesis objectives

The primary objective of this thesis is to evaluate the potential of the existing hydraulic plant at the Hydraulics and Fluid Mechanics Laboratory of Polytechnic University of Turin to generate orifice-induced hydrodynamic cavitation capable of disrupting robust microalgal cell walls. To this end, the study systematically characterizes the plant's hydrodynamic performance under controlled operating conditions and orifice geometries, quantifying pressure losses, cavitation number, and bubble-dynamics indicators, and relates these measurements to cell-disruption outcomes to assess feasibility and operating windows.

## 2 Literature Review

Microalgae represent a promising, sustainable biomass resource for applications in food, feed, and biofuel production, though significant techno-economic challenges, such as efficient harvesting and cell disruption methods, still exist. (Waghmare et al., 2019)

Cavitation pretreatment—whether induced hydrodynamically or acoustically—offers a sustainable, solvent-free means of disrupting microalgal cell walls by generating and collapsing microbubbles that create localized shear forces and transient hotspots ,thereby improving access to intracellular lipids, proteins, carbohydrates and carotenoids while preserving their bioactivity.(Sumeru et al., 2025)

## 2.1 Microalgae Structure and Lysis Techniques

Microalgae is a general term for microscopic, photosynthetic organisms commonly found in freshwater, seawater, or soil. They are important due to their fast growth and capacity to synthesize various compounds, including bioactive substances and lipids. Microalgae are highly diverse and adapt to extreme environmental conditions thanks to their complex and protective cell walls, which can vary by species. These cell walls influence how easily intracellular contents can be extracted, affecting downstream processing steps. Their cell walls often contain polysaccharides, proteins, and even lignin, and may also include surface features or molecules that enhance binding with metal ions or other substances. (Shivakumar et al., 2024)

Galdieria sulphuraria, selected as the target species for this study, is a thermo-acidophilic microalga from the Cyanidiophyceae (Rhodophyta) class, known for its ability to thrive in extreme environments such as geothermal sulphuric springs with low pH, elevated temperatures, and high salinity. It demonstrates metabolic flexibility through autotrophic, heterotrophic, and mixotrophic growth modes, allowing it to utilize a wide range of organic

carbon sources. Notably, G. sulphuraria not only endures these harsh conditions but also synthesizes a variety of bioactive compounds. In addition, it contributes to environmental remediation by removing nutrients, pathogens, and heavy metals from wastewater, and has shown potential in recovering rare earth elements from both mining effluents and electronic waste. (Retta et al., 2024)

Cell disruption techniques are generally categorized into two main types: mechanical and non-mechanical methods. Each of these categories includes several specific techniques, which are illustrated in Figure 1 (Rahman et al., 2022).

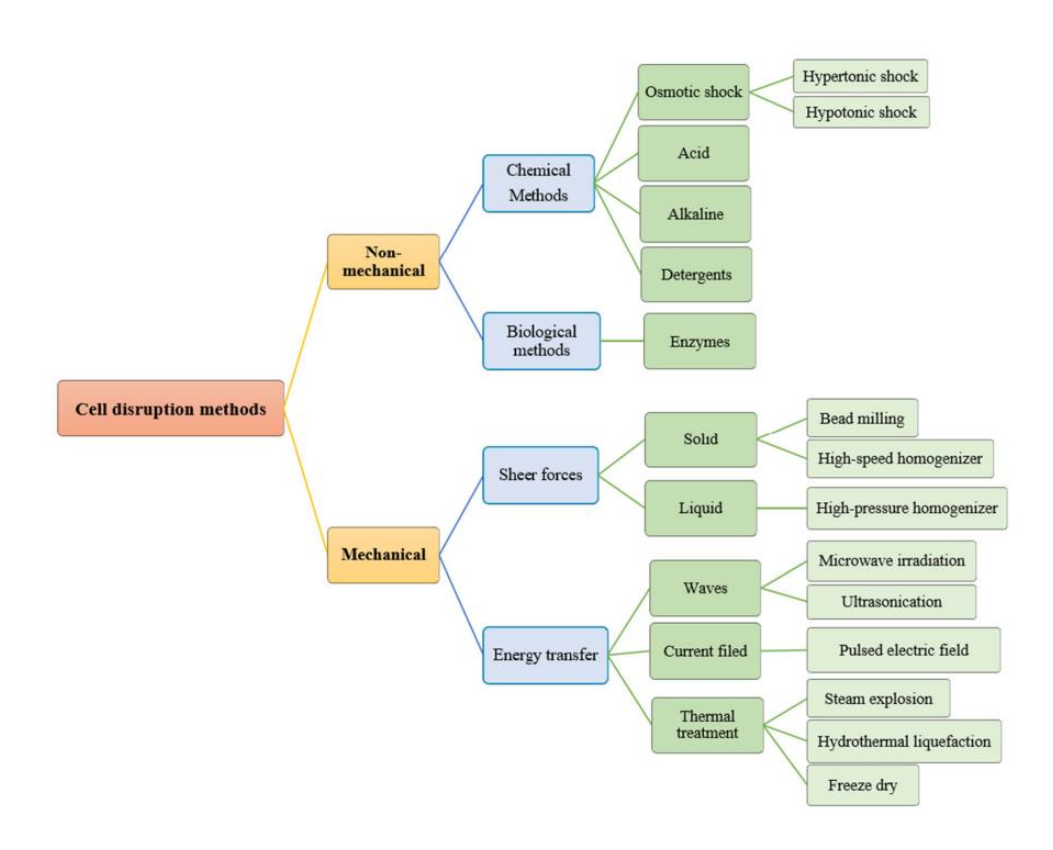


Figure 1 Different cell disruption techniques for microalgae(Rahman et al., 2022)

Conventional methods used to break open algal cells for processing—such as homogenization, microwave treatment, sonication, and bead milling—are typically energy-intensive and costly. These approaches aim to rupture the tough cell walls of algae to release valuable compounds like lipids and proteins. However, their effectiveness varies across different algal species. (Sydney et al., 2018)

On the other hand, Hydrodynamic cavitation serves as an efficient technique for breaking down microalgae cells by generating intense physical forces. These forces result from the formation, expansion, and sudden collapse of bubbles, which lead to cell wall rupture and promote the release of internal cellular contents(Arya et al., 2023). Hydrodynamic cavitation is highly effective at breaking open cell walls because the collapse of the bubbles releases an intense burst of localized energy. Although these events last only a fraction of a second, they generate extreme conditions, with rising pressures and temperatures, which are more than enough to cause severe structural disruption(Setyawan et al., 2020). A greater pressure drop and higher flow velocity intensify bubble collapse, producing mechanical forces strong enough to rupture cell walls(Save et al., 1994).

The intricate mechanical and chemical actions produced during cavitation—such as shock waves, microjets, and the formation of hydroxyl radicals—can cause severe damage to algal cells. Studies have shown that cavitation disrupts cellular structures through mechanical means like shock waves and microjets, while also producing reactive hydroxyl radicals. These radicals chemically modify proteins and lipids by oxidizing thiol groups on the cell wall and membrane, which alters membrane permeability and affects the overall function of the algal cells(Chai et al., 2025).

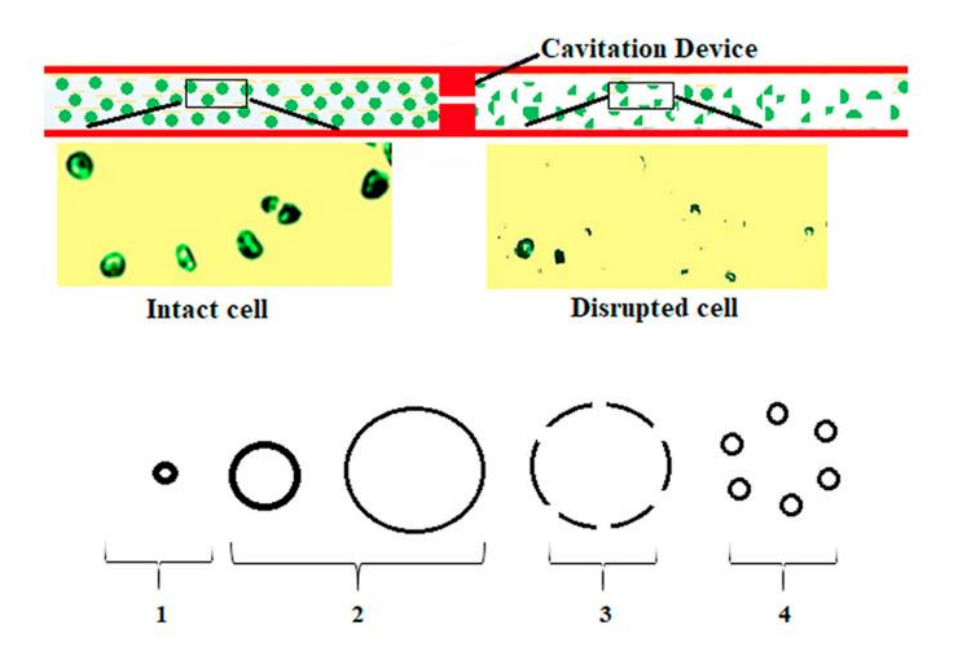


Figure 2 Mechanism of hydrodynamic cavitation (1) Generation of nuclei, (2) Expansion of bubbles to maximum, (3) Collapse of bubble, (4) Bang-release of energy. (Waghmare et al., 2019)

## 2.2 Cavitation Phenomenon

Cavitation can be defined as the breakdown of a liquid medium under very low pressures. This makes cavitation relevant to the field of continuum mechanics, and it applies to cases in which the liquid is either static or in motion(Franc & Michel, 2005). There are two primary types of cavitation based on how these pressure conditions are achieved:

Hydrodynamic Cavitation (HC) is defined as cavitation in flowing liquids. This includes flows through Venturi nozzles, in narrow passages (e.g. hydraulic valves) or around wings or propeller blades(Franc & Michel, 2005).

Acoustic cavitation occurs in a static or nearly static liquid. When an oscillating pressure field is applied over the free surface of a liquid contained in a reservoir, cavitation bubbles may appear within the liquid bulk if the oscillation amplitude is large enough. The above definition of cavitation introduces the concept of a pressure threshold, beneath which liquid microbubbles.(Franc & Michel, 2005)

## 2.2.1 Thermodynamic trigger: Vapor Pressure

Vapor pressure can best be understood using classical thermodynamics. On a phase diagram, there's a curve connecting the triple point  $T_r$  to the critical point C, separating liquid and vapor phases. Crossing this curve means the fluid undergoes evaporation or condensation at the vapor pressure  $P_v$ , which depends only on temperature T.(Franc & Michel, 2005)

Cavitation occurs by lowering pressure while keeping temperature mostly constant, which is common in real flows. Cavitation is similar to boiling, except it's driven by pressure reduction rather than temperature increase. Usually, especially for cold water, only a small amount of heat is needed to form vapor, so the temperature barely changes, and the process remains almost isothermal.(Franc & Michel, 2005)

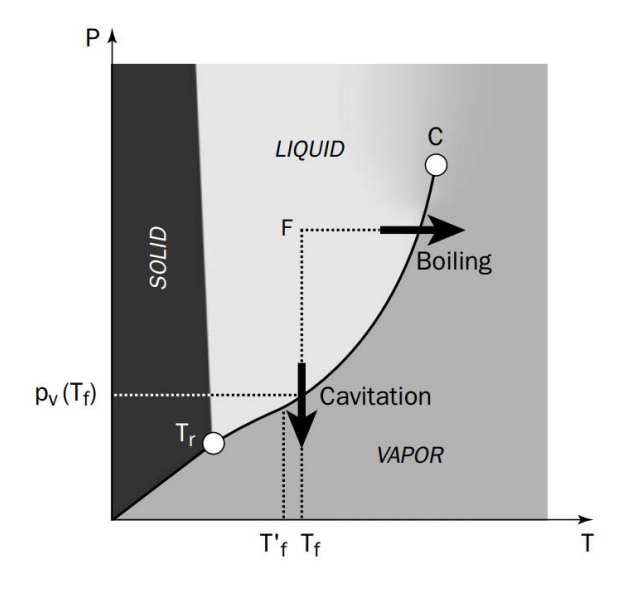


Figure 3 Phase Diagram(Franc & Michel, 2005)

From theory, cavitation initially has three steps: (a) formation of a small empty space (void creation), (b) quick filling of this space with vapor,(c) rapid saturation with vapor.(Franc & Michel, 2005)

In reality, these steps happen so quickly that the void immediately fills and saturates with vapor. It's important to understand that the vapor-pressure curve  $P_{\nu}(T)$  isn't an absolute boundary—rapid changes may cause deviations from it.(Franc & Michel, 2005)

In summary, just because local pressure equals the vapor pressure doesn't guarantee cavitation. There's typically a "static delay," meaning the actual pressure at cavitation inception is lower than the vapor pressure. Additionally, there can be a "dynamic delay," because bubbles need time to grow visibly.(Franc & Michel, 2005)

## 2.2.2 Hydrodynamic origin of low pressure

A convenient way to visualise how static pressure can fall in pipe flow is to start from the one-dimensional energy (Bernoulli) balance. For an incompressible, steady flow, the specific energy (head) at any cross-section is:

$$H = z + \frac{p}{\rho g} + \frac{v^2}{2g}$$

Where:

H is total energy head (energy per unit weight of fluid)

z is the elevation term,

 $\frac{p}{\rho g}$  is the pressure term,

 $\frac{v^2}{2g}$  is the velocity term,

between an upstream section 1 and a downstream section 2 gives:

$$z_1 + \frac{p_1}{\rho g} + \frac{v_1^2}{2g} = z_2 + \frac{p_2}{\rho g} + \frac{v_2^2}{2g} + h_f$$

with  $h_f$  the head loss due to friction. In the ideal (inviscid) limit ( $h_f = 0$ ); any local increase in velocity head must therefore be balanced by a decrease in pressure head—speed-up causes pressure-drop. In real pipelines, however, viscous dissipation converts mechanical energy into the additional head-loss term  $h_f$ . For a constant-diameter pipe, the mean velocity is uniform ( $v_1 = v_2$ ), so the equation becomes:

$$p_2 = p_1 + \rho g(z_1 - z_2 - h_f)$$

Here, the friction term appears directly as a further drop in pressure head. energy loss becomes a pressure drop(Munson et al., 2013). Whether the pressure depression is produced by a velocity spike or by cumulative head loss, cavitation can begin once the minimum absolute pressure equals the liquid's vapour pressure.

## 2.2.3 Definition and Types of Nucleation

Vaporization in liquids typically starts at free surfaces—like those on gas bubbles or solid particles—which act as initiation sites for cavitation and are referred to as "cavitation nuclei."(Zheng et al., 2022).

The initiation of cavitation occurs at microscopic weaknesses, which represent areas with reduced liquid cohesive strength that allow vapor cavities to form easily.(Brennen, 2013)two types of nucleation has been defined as:

Homogeneous nucleation: occurs when thermal motion in a clean liquid creates short-lived nanometre-scale voids. The voids transform into macroscopic bubbles when the surrounding pressure reaches a specific low threshold(Brennen, 2013).

Heterogeneous nucleation: In practice, the dominant initiation sites are found at solid—liquid interfaces (e.g., container walls, valve surfaces) or on suspended particles and pre-existing microbubbles. The energy barrier for phase separation becomes lower at interfacial imperfections, which leads to preferential rupture and bubble growth at these sites.(Brennen, 2013)

## 2.2.4 Bubble Dynamics

After initiating cavitation, these cavities, or bubbles, subsequently grow due to the pressure difference between the inside and outside of the bubbles(Blake, 2017).

The dynamics of bubbles are complex and are associated with a variety of factors, including surface tension, viscous effects, and noncondensable content(Zheng et al., 2022)

The growth can be further influenced by factors such as gas diffusion into the bubble and heat transfer across the bubble interface (Blake, 2017). Numerical models, like the Rayleigh-Plesset equation, describe the bubble radius over time, considering liquid properties such as viscosity and surface tension. (Brennen, 2013)

Bubbles expand whenever the local pressure drops below the liquid's vapour pressure, and they collapse once the pressure rises above that level again. If a bubble collapses close to a solid surface, it can shoot out a fast liquid jet and release shock waves, both of which strike the wall with very high pressures.(Sarkar et al., 2021)These features have been identified as the main source of cavitation erosion and responsible for severe structural damages(Phan et al., 2022)

## 2.3 Hydrodynamic Cavitation (HC)

Hydrodynamic cavitation can be easily produced when a liquid flows through a constriction such as a throttling valve, orifice plate, or Venturi tube. As the liquid passes through this narrowing, its velocity increases due to the conversion of pressure energy into kinetic energy. If the reduction in pressure at the narrowest point (typically the vena contracta) is sufficient to drop below the cavitation threshold—generally the vapor pressure of the liquid at operating temperature—numerous vapor cavities are formed. As the flow continues and pressure recovers downstream, these cavities rapidly collapse. With careful system design, the collapse of cavitation bubbles under hydrodynamic conditions can be made to closely mimic the conditions seen in acoustic cavitation. This enables a range of practical applications that were traditionally achieved through acoustic cavitation, but with significantly lower energy requirements than those in sonochemical reactors (Gogate & Pandit, 2005).

#### 2.3.1 Cavitation Number

The following description of cavitation number and pressure coefficient is adapted from Brennen (2013), who provides a comprehensive theoretical framework for cavitation inception in flowing liquids. In order to understand how cavitation begins in a flowing liquid, it is essential to examine how pressure behaves throughout the flow field. A key concept for this analysis is the pressure coefficient  $C_p$ , a dimensionless parameter that expresses the deviation of local static pressure from a reference free-stream pressure. It is defined as:

$$C_P(x_i) = \frac{P(x_i) - P_{\infty}}{1/2 \rho U_{\infty}^2}$$

Where  $P(x_i)$  is the local static pressure at that point,  $P_{\infty}$  is the reference pressure in the free stream,  $\rho$  is the liquid density,  $U_{\infty}$  is the free-stream velocity. In any flow field, there is usually a location where the pressure reaches its minimum—this point is represented by  $C_{Pmin}$ . A more negative  $C_P$  value implies a deeper pressure dip, and  $C_{Pmin}$  helps identify where cavitation is most likely to occur.

To predict whether cavitation will initiate, another useful dimensionless quantity is the cavitation number. The cavitation number  $C_v$  is a dimensionless parameter that indicates the potential for cavitation to occur in a flowing liquid. It is defined as:

$$C_v = \frac{P_{\infty} - P_v(T_{\infty})}{1/2 \rho U_{\infty}^2}$$

where  $P_{\infty}$  is the Free-stream (reference) pressure of the liquid,  $P_{\nu}(T_{\infty})$  is the Vapor pressure at the same temperature,  $U_{\infty}$  is the reference flow velocity, and  $\rho$  the liquid density. The cavitation number measures how close the flow conditions are to producing cavitation. Lower values of  $C_{\nu}$  indicate a higher chance of cavitation. In an ideal fluid, cavitation begins precisely when the cavitation number equals the negative of the minimum pressure coefficient:

$$C_{vi} = -C_{Pmin}$$

This condition marks the incipient cavitation number  $C_{vi}$ , at which vapor bubbles first start to appear. However, in real fluids, effects like surface tension, impurities, and the finite time required for bubbles to grow can shift the actual onset of cavitation, making the observed  $C_{vi}$  slightly different from the theoretical value. Despite these deviations, the relationship between  $C_P$  and  $C_v$  offers a reliable framework for identifying when and where cavitation is likely to occur in hydrodynamic systems.

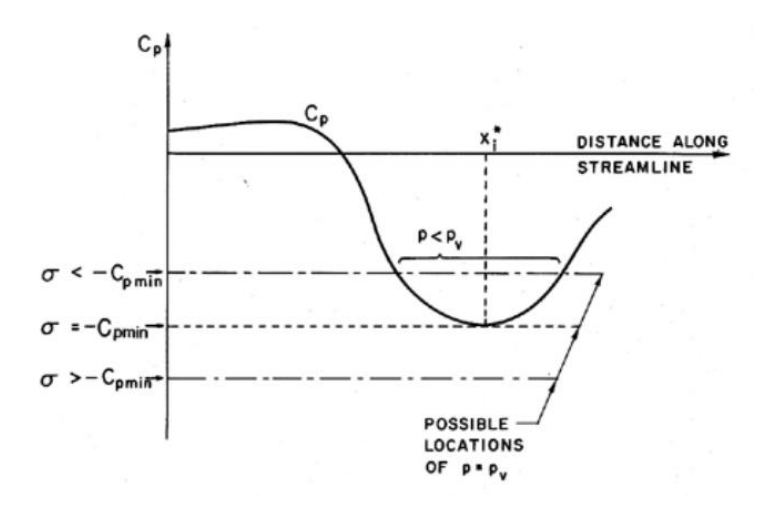


Figure 4 Schematic of pressure distribution on a streamline(Brennen, 2013).

## 2.4 Reactor Designs for Hydrodynamic Cavitation

Hydrodynamic cavitation, created by directing liquid flow under controlled conditions, has been explored in recent years as an alternative to acoustic cavitation. This approach has proven to be more efficient for large-scale applications. (Moholkar & Pandit, 2001)

A Hydrodynamic Cavitation Reactor (HCR) is a system designed to intentionally generate cavitation in a controlled environment and harness the energy from bubble collapse for physical or chemical processes. HCRs can function as standalone units or be integrated into industrial systems. (Zheng et al., 2022).

There are two main types: stationary and rotational HCRs. Stationary HCRs use simple constrictions like venturi tubes or orifice plates to increase fluid velocity, creating low-pressure zones where cavitation forms. Their straightforward design makes them popular for lab-scale studies. (Zheng et al., 2022)

To better understand and optimize the design of hydrodynamic cavitation reactors (HCRs), Moholkar and Pandit conducted numerical simulations on two common flow geometries: Venturi tubes and orifice plates. Their study, based on a nonlinear continuum mixture model, highlighted the distinct nature of bubble dynamics in each configuration. In Venturi-based flows, bubbles exhibited stable oscillatory motion due to a linear pressure recovery, while in orifice flows, the interaction of a sharp pressure drop and oscillatory turbulent gradients led to a combination of stable and transient bubble motion, similar to acoustic cavitation. This resulted in significantly higher cavitation intensity in orifice setups. Based on these observations, the authors proposed design strategies: Venturi geometries are more suitable for moderate cavitation applications, while orifice configurations are better for processes requiring intense cavitation. Parameters such as the constriction length, diameter ratios, and downstream pipe sizing were shown to play critical roles in controlling cavitation performance. (Moholkar & Pandit, 2001). The process of cell disruption in microalgae lysis requires high cavitation intensity because it produces the necessary forces needed to break cell walls (Waghmare et al., 2019).

The present study selects the orifice configuration because its higher cavitation intensity makes it more appropriate for cell disruption applications.

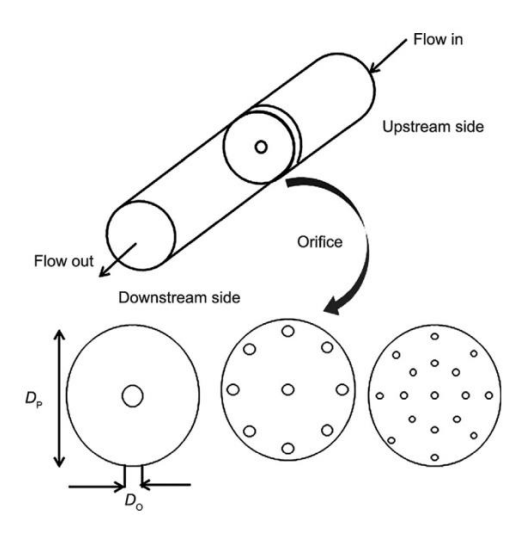


Figure 5 Illustration of a different orifice design. DO: diameter of orifice; DP: diameter(Zheng et al., 2022)

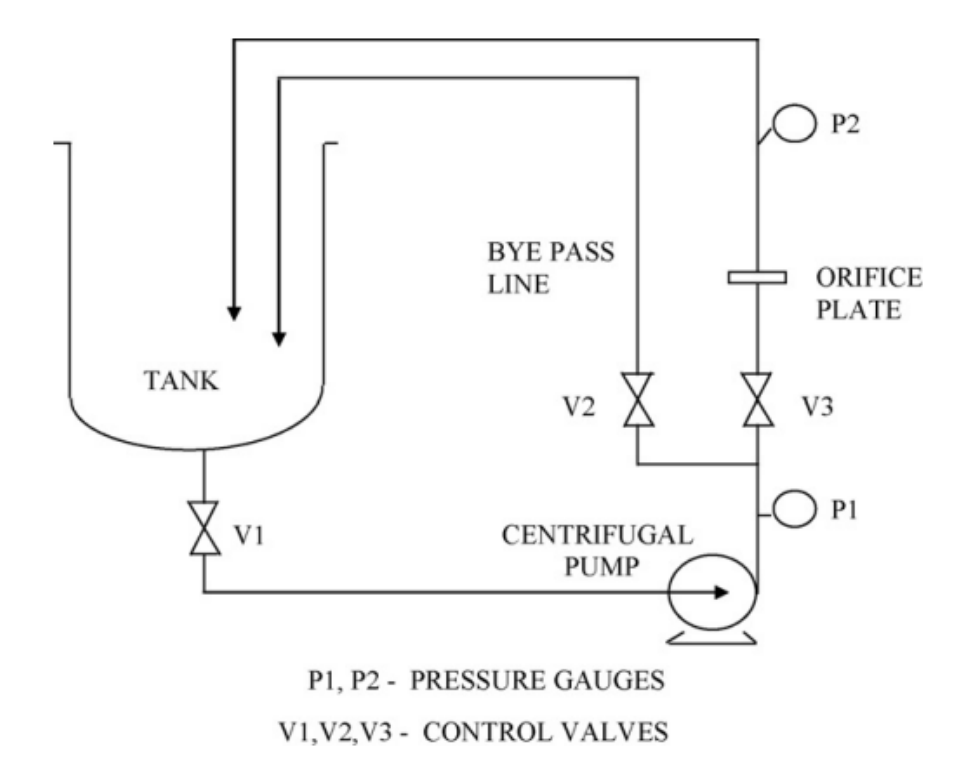


Figure 6 Orifice plate hydrodynamic cavitation setup.(Gogate & Kabadi, 2009)

### 2.4.1 Head Loss in Orifice Plates

Orifices introduce localized cross-sectional reductions in pipelines, causing pressure drops and energy dissipation. The head losses produced by an orifice depend largely on its geometry (Adam et al., 2019)

As fluid accelerates through orifice holes, the local pressure can drop below the vapor pressure, forming vapor bubbles that collapse downstream, releasing energy in the form of noise, vibration, and potential damage to pipe walls. These effects increase as the cavitation number decreases, especially in the fully cavitating regime, where constant bubble generation leads to sustained energy loss.(Maynes et al., 2013)

Pressure loss is defined as the permanent drop in static pressure between two specific wall locations in the pipe: one upstream of the orifice plate—where the approach-flow impact pressure is still negligible—and another downstream of the plate, where the jet's expansion is considered fully complete and static pressure has finished recovering. The loss coefficient k quantifies the ratio of pressure loss to kinetic energy per unit volume (ISO 5167-2, 2003).

In the context of local pressure losses such as those caused by orifices, the use of a fluid-resistance coefficient provides a standardized method to quantify energy dissipation. the head loss coefficient (denoted as k) expresses the ratio of the pressure loss  $\Delta H$  to the dynamic pressure  $v^2/2g$  at a given flow section. This dimensionless parameter allows to accounting for head losses caused by geometric disturbances in the pipe—like sudden contractions or expansions—by relating them to the kinetic energy of the fluid. this formulation simplifies the evaluation of flow resistance in fittings and singular elements, offering a consistent basis for hydraulic analysis(IDELCHIK, 2008). The head loss coefficient is a key parameter in orifice-based energy dissipators, directly influenced by the contraction ratio (orifice diameter to pipe diameter) and the thickness ratio(orifice thickness to pipe diameter). A lower contraction ratio leads to higher head loss. The Reynolds number has minimal effect on head loss above the value of  $10^5$ (Jianhua et al., 2010).

In hydraulic systems, controlling flow is primarily done by restricting it through valve orifices. These systems are typically represented using lumped parameter models. The standard orifice flow equation, derived from Bernoulli's principle, links flow rate to the orifice area and the square root of the pressure difference, with a proportionality factor known as the discharge coefficient  $C_d$  (Wu et al., 2002). The discharge coefficient is a dimensionless parameter defined as the ratio between the real volumetric flow rate passing through a restriction and the ideal flow rate predicted for that restriction. It is commonly used to describe how nozzles and orifices influence flow characteristics and associated pressure losses in fluid systems(Essien et al., 2019). This coefficient is often assumed to

be constant and independent of the Reynolds number (Wu et al., 2002). However, at very small orifice openings,  $C_d$  can change significantly, making this assumption inaccurate and potentially leading to large modeling errors.

The discharge coefficient varies with both flow conditions and nozzle geometry. It is primarily influenced by the Reynolds number and by geometric ratios such as length-to-diameter and diameter ( $\beta$ ) ratios. Additional geometric factors—particularly the sharpness of the upstream edge in orifice-type nozzles and the pipe cross-section housing the nozzle—also significantly affect  $C_d$ . While the discharge coefficient changes noticeably at low Reynolds numbers (laminar flow), its dependence on Re becomes negligible once the flow is fully turbulent (Re >  $10^4$ ). (Essien et al., 2019)

In an orifice, the discharge coefficient stays high while the flow is single-phase; once cavitation begins, the formation of vapor pockets and added turbulence constrict the effective throat, so the coefficient drops, and it falls even more abruptly if cavitation evolves into hydraulic flip.(Chemloul, 2012)

# 2.5 Cavitation Intensity Requirements for Microalgae Cell Wall Rupture

Cavitation tends to initiate when the cavitation number falls below a certain threshold, typically around 1 or less, as reported in several studies.(Sumeru et al., 2025)

Different species have varying cell wall structures, affecting the cavitation energy required for disruption. (Greenly & Tester, 2015). The stress provided by the cavity collapse should be higher than the cell wall strength of the microbes to break the cell wall (Carpenter et al., 2017)

Applying hydrodynamic cavitation to inactivate *Scenedesmus* microalgae achieved a maximum efficiency of 85% at a cavitation number of 0.17 after 60 minutes of treatment.

This demonstrates that lower cavitation numbers, combined with sufficient exposure time, lead to more effective microalgae inactivation.(Batista et al., 2017)

Wu et al. (2012) investigated the influence of orifice plate diameter and cavitation device placement on blue-green algae removal. Their results showed that under suction conditions, using a 12 mm orifice, a maximum removal efficiency of 20% was achieved at a cavitation number of 0.54 and an inlet pressure of 0.063 MPa. This highlights the impact of cavitation number and orifice geometry on the cell disruption performance of hydrodynamic cavitation systems.(Carpenter et al., 2017)

According to Bashir et al. (2011), the geometry of a cavitating device plays a critical role in determining its efficiency. Key performance factors—including the number of cavities generated, their residence time in the low-pressure region, the rate of pressure recovery downstream, cavity trajectory, and overall cavitation intensity—can all be controlled through geometrical design optimization.(Carpenter et al., 2017)

for most applications—including wastewater treatment, microbial inactivation, and emulsification An optimal Cv range between 0.1 and 0.3 is recommended. Furthermore, higher inlet pressures are beneficial but must be balanced with device geometry to avoid excessive energy consumption. (Carpenter et al., 2017)

The extraction of lipids from *Nannochloropsis sp.* using hydrodynamic cavitation in a batch system with a methanol–hexane solvent mixture showed that the optimum cavitation number for efficient lipid extraction was 0.126, under which the lipid yield increased significantly with rising specific energy until a plateau was reached. The optimal extraction temperature was 42 °C, and the minimum energy required for extraction was 16.743 MJ/kg lipid, obtained at a solid concentration of 0.105 g/g. These findings confirm the potential of HC for reducing the energy cost of microalgal biodiesel production when operated under optimal cavitation intensity and process conditions.(Budiman, 2018)

hydrodynamic cavitation achieved effective microalgae cell disruption at a cavitation number of ~0.125, with an energy requirement of 3 MJ/kg for lipid extraction—about ten

times lower than sonication (46.8 MJ/kg). The process was most efficient within 4 minutes, with disruption mainly occurring at the cell wall, enabling solvent penetration. This highlights HC's suitability for energy-efficient biofuel production. (Lee et al., 2015)

## 3 Materials and Methods

## 3.1 Experimental Facility Description

The experimental setup and equipment used during the tests are explained in this chapter. The majority of experiments were performed using a hydraulic circuit specifically designed to investigate hydrodynamic cavitation phenomena and their various applications at the cavitation lab of the Department of Environment, Land and Infrastructure Engineering, Politecnico di Torino..

## 3.1.1 Hydraulic Circuit

The experimental facility received special design and assembly to analyze the hydrodynamic cavitation. The system operates in a closed circuit configuration with primary components made of AISI 316L stainless steel that meet sanitary requirements and shows resistance to corrosion. Standardized DIN-11851 flanged or threaded fittings connect individual pipeline components to ensure easy assembly and disassembly as well as sterilization between experiments. The core component of the circuit contains a transparent cylindrical observation chamber with a perforated orifice plate, which serves as the cavitation reactor. High velocity flow through a narrow orifice causes a sudden pressure drop, which can lower the local pressure below the vapor pressure of water. This induces localized boiling and the formation of vapor bubbles. As the fluid continues downstream and pressure recovers, these bubbles collapse violently, leading to hydrodynamic cavitation. The hydraulic setup integrates two main subsystems:

Primary Hydraulic Loop: The system includes four identical funnel-shaped reservoirs that create a total storage volume of approximately 30 liters, which provides both fluid supply and continuous circulation during testing. The circuit maintains fluid circulation through a centrifugal pump, which operates at 2853 RPM under 25 bar pressure. The cavitation

reactor area is equipped with two pressure sensors, which measure fluid pressure upstream and downstream of the orifice. A ball valve operated by hand exists downstream of the reactor to control the outlet pressure, which enables the adjustment of the cavitation number to experimental values. A dedicated sampling valve located downstream allows operators to collect treated fluid samples before further analysis.

Cooling System Loop: A chiller unit paired with an immersed coil within the reservoir operates as an independent cooling system to maintain stable fluid temperatures throughout extended experimental runs, which minimizes temperature fluctuations that could affect experimental results. The ISO-standard piping in the circuit maintains wall thicknesses from 1.8 mm to 2.2 mm. The entire experimental setup rests on a robust steel scaffolding frame with a wooden base, which provides structural stability and easy accessibility and includes a protective plexiglass cover for cleaning and disinfection processes.

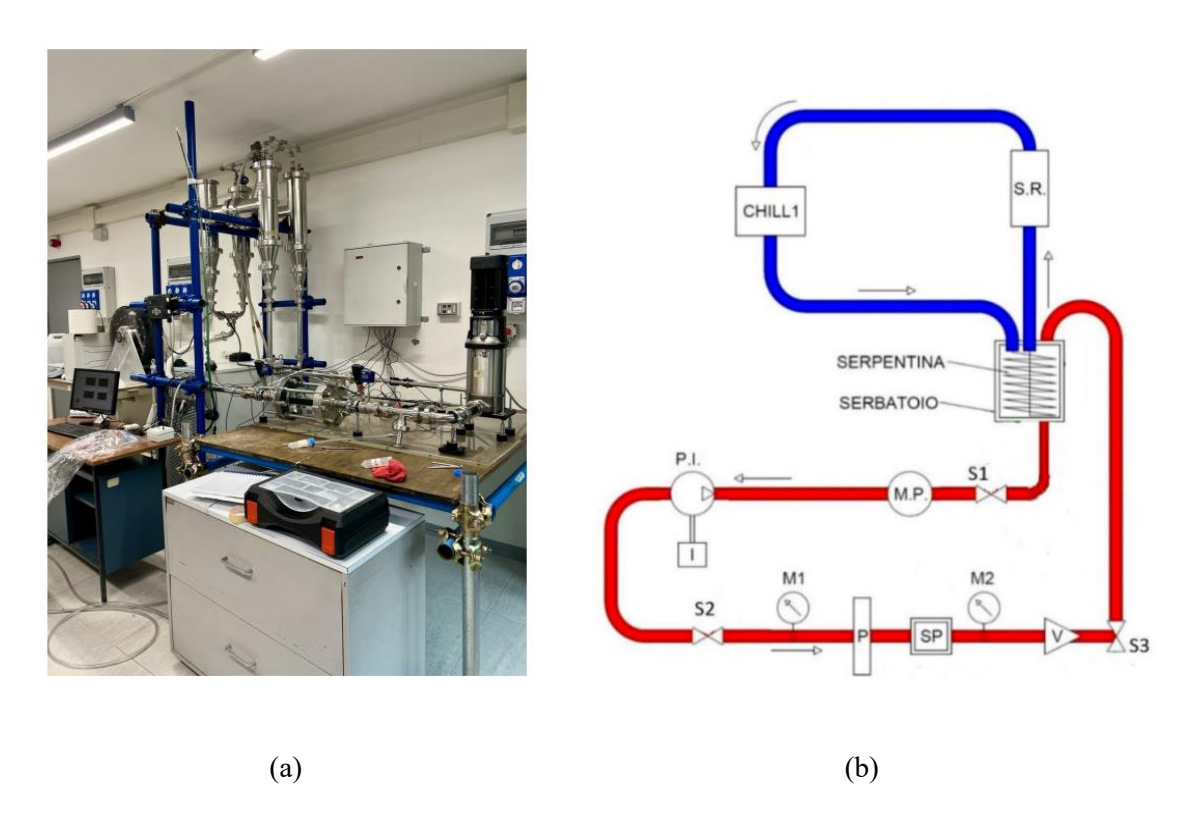


Figure 7 (a) Experimental hydraulic circuit setup. (b) Schematic of the hydraulic circuit

The pump (P.l.) accelerates the flow and reaches the perforated plate (P). The glass observation window (SP) allows observation of cavitation effects. The manometer (M1) measures the downstream pressure, and the ball valve (V) controls the downstream pressure (M2). the flow rate is measured by the flow meter (M.P.). The drains (S1, S2) are closed to prevent water leakage.



Figure 8 Transparent cavitation chamber

## 3.1.2 High-speed camera

The Photron FASTCAM Nova S16 high-speed camera (model 1100K-M-128GB, 10GbE version) served as the tool to observe cavitation phenomena within the hydraulic test circuit. The camera used a long focal Nikon lens, which was mounted on a tripod to maintain image stability and proper alignment with the observation window of the cavitation reactor. The high-speed imaging system recorded cavitation bubble formation and collapse because these events occur at microsecond timescales, which standard video equipment cannot detect. The system operated at maximum frame rates of 50,000 frames per second (fps) to provide direct observations of cavitation intensity during different flow and pressure conditions. The high temporal resolution allowed to obtain reliable images of fast-evolving microbubbles and their collapse dynamics. The visual data served as a critical

tool to evaluate the effects of cavitation on microalgae cell wall disruption while providing essential information about treatment process effectiveness.



Figure 9 High-speed camera setup (Photron FASTCAM Nova S16) used for cavitation bubble observation.

## 3.2 Evaluation of Methods to Lower Cavitation Number

The reduction of cavitation number stands as a crucial factor for increasing cavitation event intensity. The formation of powerful vapor bubbles and forceful collapses becomes more likely when the cavitation number decreases, as this process is essential for cell disruption treatments that require bubble collapse to break cell walls. Two main approaches were examined to reduce the experimental system's cavitation number. The cavitation number is defined as:

$$C_v = \frac{P_2 - P_v}{1/2 \rho v^2}$$

Where (P2) is the downstream pressure, (Pv) the vapor pressure of the fluid, and (v) the bulk flow velocity in the orifice.

As the equation indicates, increasing the flow velocity leads to a significant reduction in cavitation number, which results in more intense cavitation activity.

The first evaluated option involved adding an additional pump to the hydraulic system. The addition of a second pump would generate a significant increase in flow rate, which produces elevated velocities and Reynolds numbers that decrease the cavitation number while strengthening bubble formation and collapse. The solution was not feasible because of operational complexity.

The second approach involved changing the orifice plate diameter. The first orifice plate used had a diameter of 4.5 mm. The study used orifice plates with different diameters to examine the relationship between orifice size, cavitation number, cavitation intensity, and bubble characteristics. The orifice diameter variation allowed to create different localized flow restrictions and velocity variations, which enabled the study of cavitation efficiency and its effectiveness on microalgae lysis under controlled operational conditions.

## 3.2.1 Pump Configuration

The theoretical evaluation showed that a second pump would enhance flow rates and decrease the cavitation number, but this solution became impractical because of operational restrictions and system limitations. The experimental campaign continued with a single-pump setup, achieving optimal operating conditions. The research concentrated on decreasing the cavitation number through modifications of the orifice diameter instead.

## 3.2.2 Orifice Plates

The research on hydrodynamic cavitation effects utilized four interchangeable stainless-steel orifice plates, which had diameters of 2 mm, 3 mm, 4.5 mm and 6 mm. The experimental setup included a design feature that made it possible to replace the perforated plates in the cavitation reactor for systematic testing under consistent hydraulic conditions. The different orifice plates created distinct flow restrictions, which produced various pressure drops that initiated cavitation. The research evaluated how different orifice diameters affected pressure dynamics and cavitation intensity.



Figure 10 Stainless-steel orifice plates with different diameters (2 mm, 3 mm, 4.5 mm, and 6 mm) used to induce cavitation in the reactor.

#### 3.3 Analytical Methods and Data Collection

The following section explains the analytical methods used to evaluate essential hydrodynamic cavitation parameters. The hydraulic circuit contained digital manometers and flowmeters, which monitored and recorded pressure differentials and flow rates. The bubble dynamics were recorded through high-speed imaging, and microscopic examinations were performed on collected algal samples to evaluate cell wall integrity. The cavitation number was determined from measured pressures and flow conditions to evaluate the efficiency of algae lysis processes under different experimental conditions.

The tests were performed at 15 fixed frequencies for each orifice plate to obtain systematic measurements of flow rates and upstream and downstream pressures, and flow velocities in each orifice. The downstream pressure was kept at atmospheric pressure to calculate the pressure differential ( $\Delta P$ ) across each orifice. The fundamental hydraulic relationship was used to calculate head loss for each plate through pressure differential:

$$H = \frac{\Delta P}{\rho g}$$

where  $(\rho)$  is the fluid density, and (g) is gravitational acceleration.

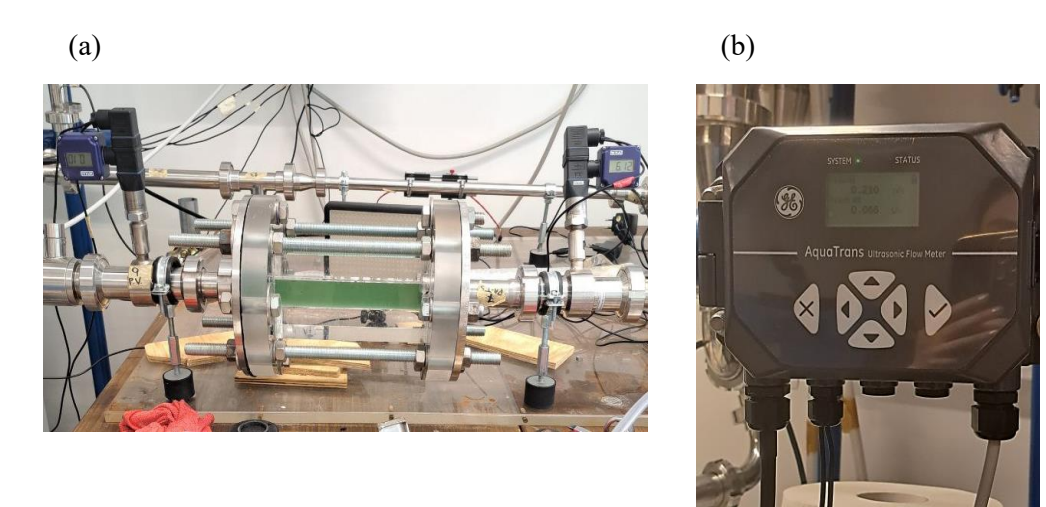


Figure 11 (a) upstream and downstream pressure gauges installed on both sides of the cavitation chamber, used to measure differential pressure across the orifice plate. (b)

Ultrasonic Flow Meter used for real-time measurement of flow rate in the hydraulic circuit.

The head loss of each perforated plate was further analyzed using the relation:

$$H = k \frac{v^2}{2g}$$

where (k) is the pressure loss coefficient specific to each orifice configuration, and (v) is the flow velocity through the orifice. The initial tests were conducted using tap water to determine head loss and calculate cavitation numbers for each orifice plate before adding the algae suspension, which provided a reliable reference to represent the actual experimental conditions.

The main objective of the initial hydraulic measurements was to understand system behavior and identify the optimal hydrodynamic conditions for enhancing microalgae cell lysis. Two key parameters were investigated: the cavitation number and vapor bubble size, as both influence the intensity and mechanical effectiveness of cavitation. High-speed imaging was used to qualitatively evaluate bubble formation and collapse.

Lower cavitation numbers are theoretically associated with more intense cavitation because they indicate a greater pressure drop relative to the fluid's vapor pressure, promoting vapor bubble nucleation and collapse. The mechanical impact on microalgae cell walls is enhanced when larger vapor bubbles collapse, as they release higher energy levels.

However, selecting an orifice diameter presents a trade-off. Small orifices generate higher flow velocities, which reduce the cavitation number and increase the likelihood of initiating cavitation. Nevertheless, very small orifices also introduce limitations that restrict bubble growth. These include shorter residence time within the low-pressure region, rapid downstream pressure recovery, and increased energy losses due to turbulence and heat dissipation. These factors collectively reduce bubble size and limit the intensity of their collapse, thereby diminishing their effectiveness in disrupting algal cell walls.

Conversely, larger orifices promote the formation of bigger vapor bubbles capable of more forceful collapse, but fail to produce low cavitation numbers due to insufficient flow acceleration. Therefore, identifying an optimal orifice diameter requires balancing two competing factors: achieving low cavitation numbers to initiate cavitation and generating large vapor bubbles to maximize collapse intensity. Several orifice diameters were experimentally tested to determine the most effective configuration for promoting microalgae lysis based on this trade-off.

# 3.4 Preliminary Manual Cavitation Test in Sealed Glass Chamber

The initial stage of the research involved a basic manual cavitation test designed to evaluate whether cavitation could be effectively generated and observed in mixtures of water and *Galdieria sulphuraria* algal suspensions. The test aimed to assess if the altered physical properties of the algae—water mixture would still allow cavitation events to occur. While this manual approach did not permit quantitative measurements such as pressure differentials or cavitation number, it provided important qualitative insights.

The setup used a sealed glass chamber placed inside a durable protective cylinder to ensure safety and prevent leakage or damage during impact. The cavitation was manually induced by striking the top of the chamber with a hammer to create localized pressure variations capable of initiating vapor bubble formation. The test began with pure water, and algae with a concentration of 6 g/L was gradually added into the 300 mL chamber. As the concentration increased, the mixture became progressively darker, which significantly affected the ability to visually track bubble dynamics through the camera. The Photron FASTCAM Nova S16 high-speed camera was used to capture bubble formation, growth, and collapse. In higher concentrations, the bubbles could no longer be visually confirmed due to the opacity of the fluid, although the characteristic "pop" sounds of collapsing bubbles remained clearly audible. These observations confirmed that cavitation could still occur in algal suspensions despite altered fluid properties, supporting the feasibility of cavitation-based treatments for such mixtures. The manual test provided preliminary confirmation that algae—water mixtures could support bubble formation, and that audio-based cues could complement visual diagnostics in cases of low visibility.

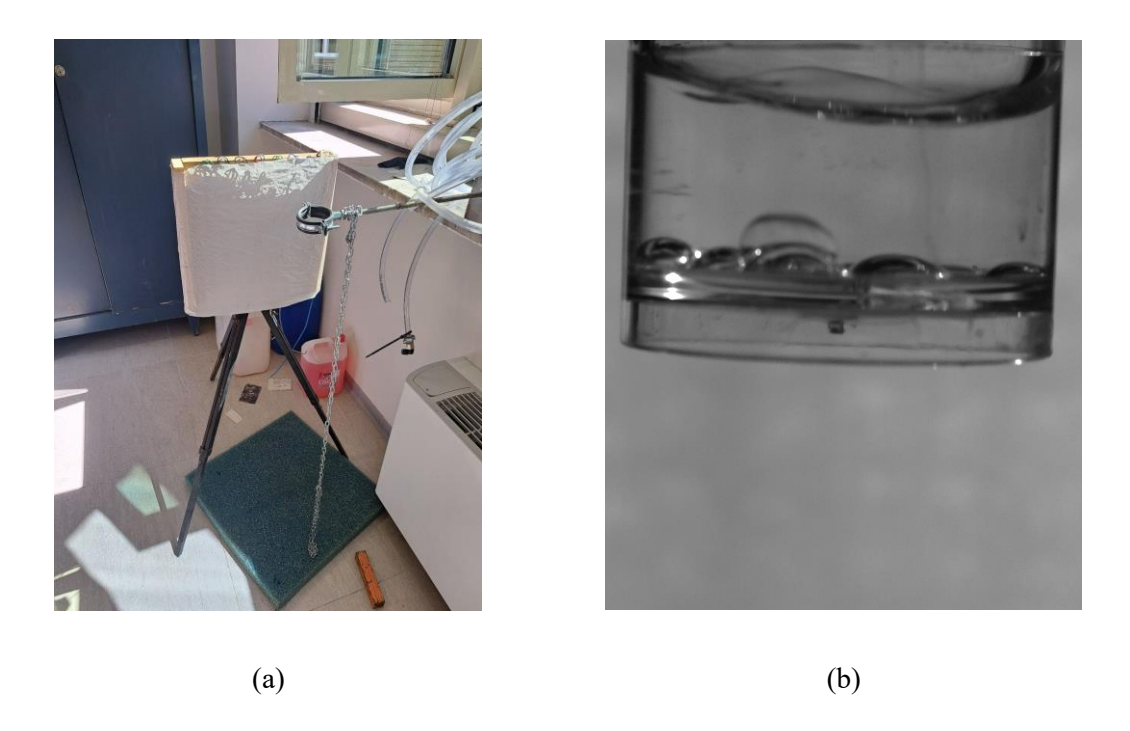


Figure 12 (a) Manual cavitation test setup with a sealed glass chamber (b) Bubble Formation

During Manual Cavitation Test

## 3.5 Algae Preparation for Hydrodynamic Cavitation

The research employed *Galdieria sulphuraria* as a unicellular red alga because of its strong cell walls and robust nature (Retta et al., 2024) to examine hydrodynamic cavitation effectiveness for algae cell wall disruption. The initial algal suspension contained 1 liter of 6 g/L concentration, which was diluted with 27 liters of tap water to achieve a circulating system concentration of 0.214 g/L. The prepared 28-liter suspension entered the hydraulic circuit while maintaining a temperature of 23°C throughout the experimental period. The integrated cooling system (chiller) stabilized temperatures to maintain steady hydrodynamic conditions and prevent temperature fluctuations that would affect fluid viscosity and algal responses during testing.

The hydraulic system operated at its maximum frequency (50 Hz) to generate a flow rate of 0.093 L/s using the smallest orifice plate diameter of 2 mm. The selected configuration

produced the minimum achievable cavitation number, which resulted in maximum cavitation intensity.

The turnover time represented the time needed for the complete fluid volume to complete one pass through the orifice, calculated as:

Turnover Time = 
$$\frac{Total\ Volume}{Flow\ rate} = \frac{28(L)}{0\ /\ 0.93(\frac{L}{s})} \approx 301(s) \approx 5\ (minutes)$$

The sampling procedure involved collecting 14 mL of circulating suspension after multiple turnovers at 10, 20, 30, and 50 treatments, which corresponded to total durations of approximately 50, 100, 150, and 250 minutes, respectively. The extracted samples from circulation maintained the same concentration level as the system at 0.214 g/L. The collected samples underwent immediate microscopic analysis after sampling to assess algal cell wall integrity changes and evaluate the potential lysis effects of hydrodynamic cavitation.

N. Of	Total	Sample
Treatments	<b>Duration(minutes)</b>	Concentration(g/L)
10	50	0.214
20	100	0.214
30	150	0.214
50	250	0.214

Table 1 Treatment duration and sample concentration for different turnover cycles of algae suspension in the hydrodynamic cavitation experiment



Figure 13 Algae Samples Collected at Different Treatment Stages

#### 4 Results and Discussions

The results and discussion are structured into two primary sections. The first part examines the hydrodynamic characterization of the experimental system by studying the relationships between head loss, cavitation number, and Reynolds number for different orifice diameters. The second part assesses the effectiveness of the hydrodynamic cavitation setup for microalgae cell disruption by analyzing cell integrity through microscopic examination after cavitation experiments.

#### 4.1 Hydrodynamic Characterization

This section provides a comprehensive assessment of the hydrodynamics associated with the cavitation reactors in terms of measured head losses and comparison with empirical estimations.

#### 4.1.1 Head Loss Coefficient

To understand the behavior of the system under various flow conditions, an analysis of energy losses across the orifice is required for both system design and cavitation performance assessment. The head loss calculation is further expressed using a dimensionless coefficient k, which is defined as:

$$H = k \frac{v^2}{2g}$$

where H is the head loss across the orifices, v is the water velocity through the orifice, and g is the gravitational acceleration. The upstream pressure  $P_u$  was measured before the orifice plate, while the downstream pressure  $P_d$  was taken as atmospheric pressure, plus

the hydrostatic head of the 1 m elevation to the pressure tap. Head loss was therefore obtained from :

$$H = \frac{P_u - P_d}{\rho g}$$

with  $\rho$  the water density at the test temperature. Based on this, the corresponding k values were subsequently calculated. These values were plotted against the Reynolds number in Figure 8.

The second plot (Figure 9) shows the head loss coefficient k against the cavitation number Cv. Since lower cavitation numbers mean a higher chance of vapor bubble formation, correlating Cv with k enables a quantitative evaluation of how head losses are affected by cavitation. Moreover, it is important for choosing configurations that might improve microalgae cell disruption.

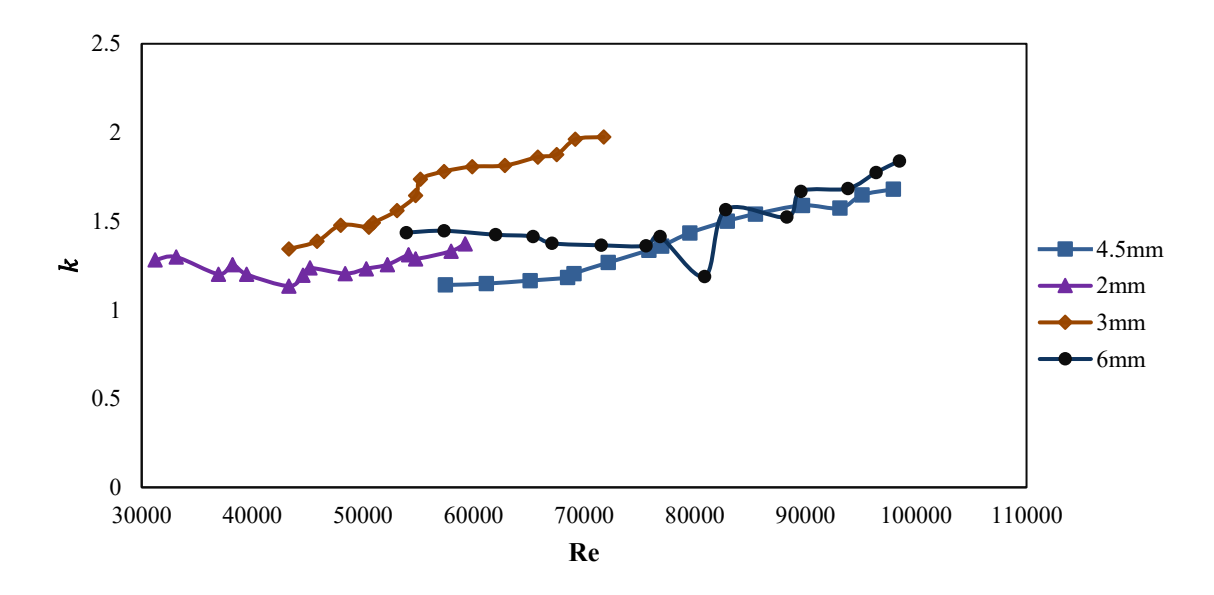


Figure 14 Variation of head-loss coefficient k with Reynolds number for the four tested orifice diameters (2 mm, 3 mm, 4.5 mm, 6 mm).

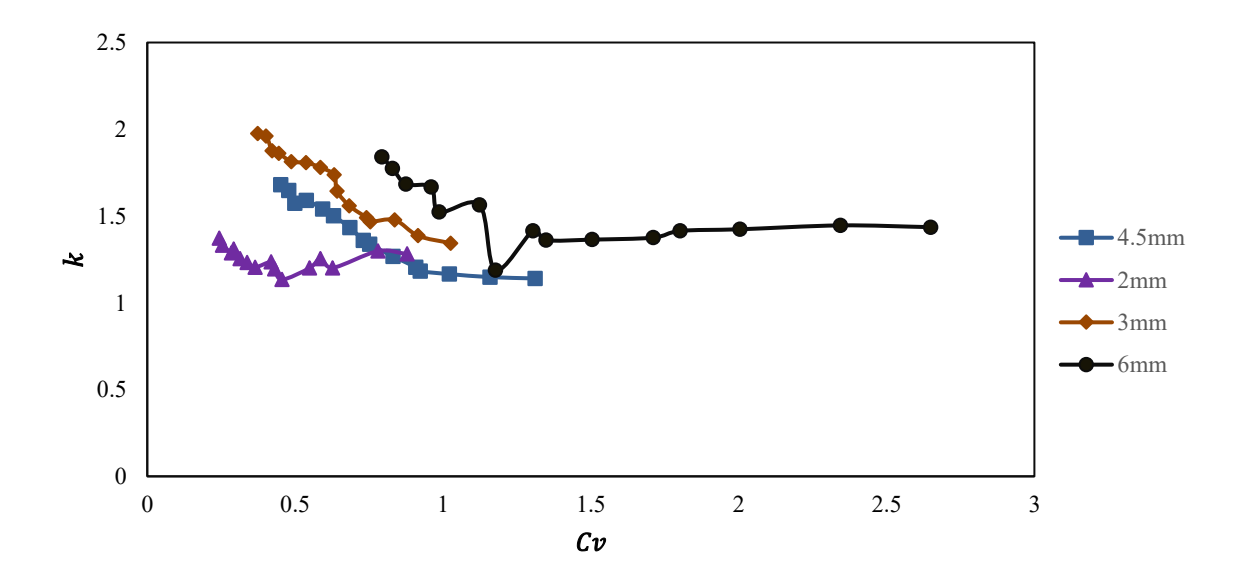


Figure 15 Head-loss coefficient k as a function of cavitation number Cv for the four orifice diameters.

According to Figure 14, the head-loss coefficient k is influenced by both Reynolds number and the orifice diameter. The 3 mm orifice produced the highest energy losses among the tested configurations, while the 2 mm orifice resulted in the lowest energy loss values. The 4.5 mm and 6 mm plates produced intermediate losses. The same data was plotted against the cavitation number in Figure 15 to investigate the relation between hydraulic behavior and cavitation onset. The k values show a significant increase when the cavitation number drops below 1, suggesting that phase-transition processes associated with the onset of cavitation contribute to the additional energy dissipation. These observations are supported by qualitative assessment of high-speed video recordings that were taken during each test. The videos showed that the 2 mm orifice, despite reaching the lowest cavitation number (Cv = 0.24), produced many small vapor bubbles, whereas larger orifices generated fewer but bigger cavities. The visual findings are consistent with the trend observed in the headloss coefficient, whereby k is dictated by a trade-off between cavitation number and bubble size. With the largest diameter, there are big bubbles choking the flow, but relatively high Cv numbers are reached. In contrast, for the smallest diameter, very low Cv numbers are reached, but with extremely small bubbles. This means that the highest head losses are reached at intermediate conditions, providing optimised conditions for low Cv and large bubbles.

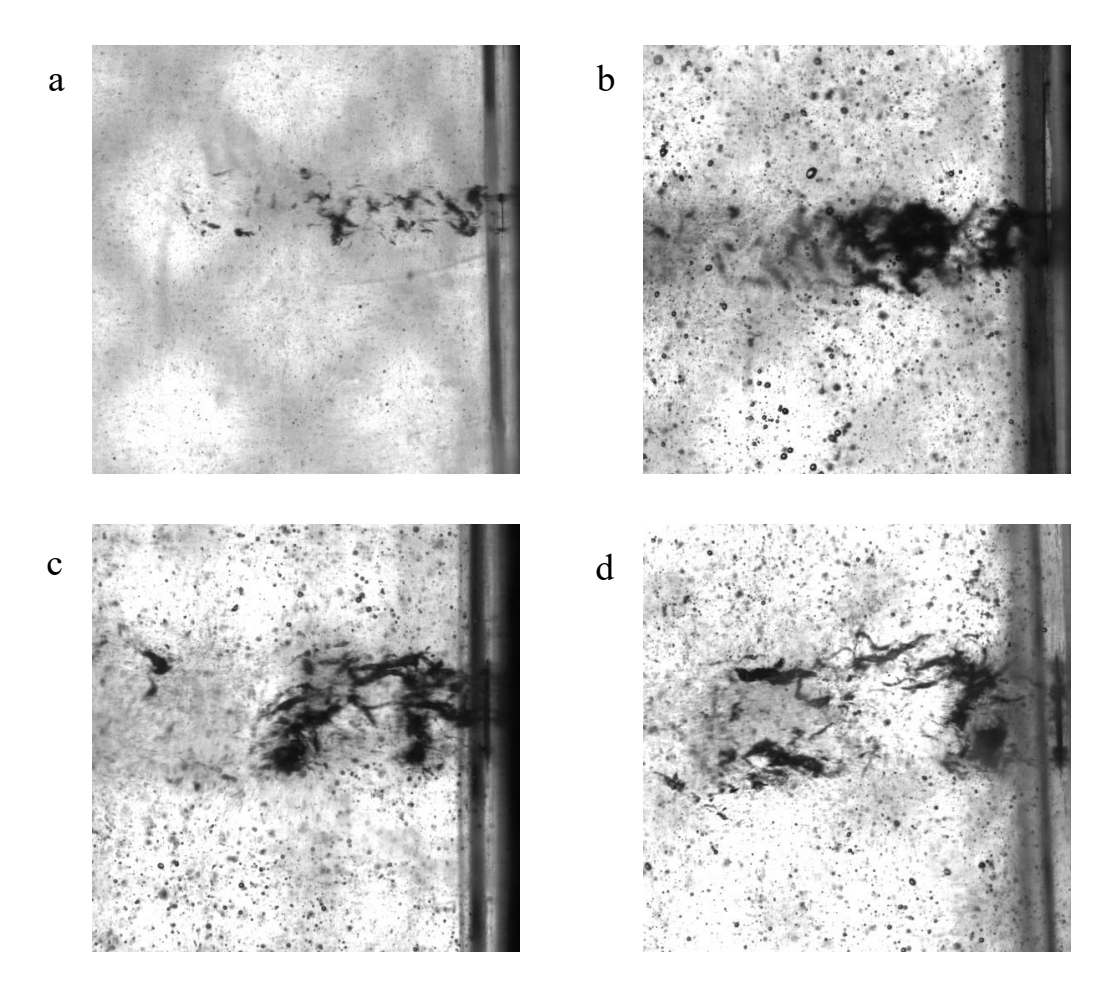


Figure 16 High-speed imaging snapshots showing cavitation bubble formation for four different orifice diameters: (a) 2 mm, (b) 3 mm, (c) 4.5 mm, (d) 6 mm.

The images highlight differences in vapor bubble size and distribution under similar flow conditions.

#### 4.1.2 Comparison of Measurements with Empirical Laws

The research evaluates whether established empirical correlations from literature match the head loss measurements collected in this study to determine their application for hydrodynamic cavitation reactor design. The empirical formulas predict the discharge coefficient  $C_d$  instead of the head loss coefficient, which provides another method to describe flow resistance. The discharge coefficient functions as a dimensionless value that

shows the relationship between actual flow rates and theoretical flow rates under equivalent conditions. Two widely used empirical models were chosen for evaluation against experimental findings:

1-Reader-Harris / Gallagher (ISO 5167) as a standard correlation developed for sharp-edged orifices :

$$C = 0.5961 + 0.0261\beta^2 - 0.216\beta^8 + 0.000521 + (0.0188 + 0.0063A)\beta^{3.5} \left(\frac{10^6 \beta}{Re_D}\right)^{0.3}$$

$$+ (0.043 + 0.08e^{-10L_1} - 0.123e^{-7L_1})(1 - 0.11A)\frac{\beta^4}{1 - \beta^4} - 0.031(M_2'^2 - 0.8M_2'^{11})\beta^{1.3}$$

Where  $D \le 71,12$  mm, the following term shall be added to the Equation :

$$+0.011(0.75-\beta)\left(\frac{2.8-D}{25.4}\right)$$

Where:

 $\beta = \frac{d}{D}$ : is the diameter ratio, with the diameters d and D expressed in millimeters

 $Re_D$  : is the Reynolds number with respect to pipe diameter D

 $L_1 = \frac{l_1}{D}$ : is the quotient of the distance of the upstream tapping from the *upstream* face of the plate

and the pipe diameter; and

 $L_2' = \frac{l_2'}{D}$  is the quotient of the distance of the downstream tapping from the *downstream* face of the

plate and the pipe diameter (L'2 denotes the reference of the downstream spacing from the downstream face, while L2 would denote the reference of the downstream spacing from the upstream face).

$$M_2' = \frac{2L_2'}{1-\beta}$$

$$A = \left(\frac{19000\beta}{Re_D}\right)^{0.8}$$

2-Swamee's empirical correlation. As a more recent empirical relation, the formulation by Swamee (2005) was developed to improve accuracy in low-Reynolds-number flows. The discharge coefficient is calculated as:

$$C_d = \{ [0.675 + 0.6\beta^2 - 0.02 \ln(Re)]^{10} + [0.5 + 0.43\beta^2]^{10} \}^{0.1}$$

For each orifice diameter (2, 3, 4.5, and 6 mm), theoretical  $C_d$  values were calculated using these models and compared against experimentally derived values  $C_{d,Exp}$ , which were obtained from pressure drop and flow rate measurements using the equation:

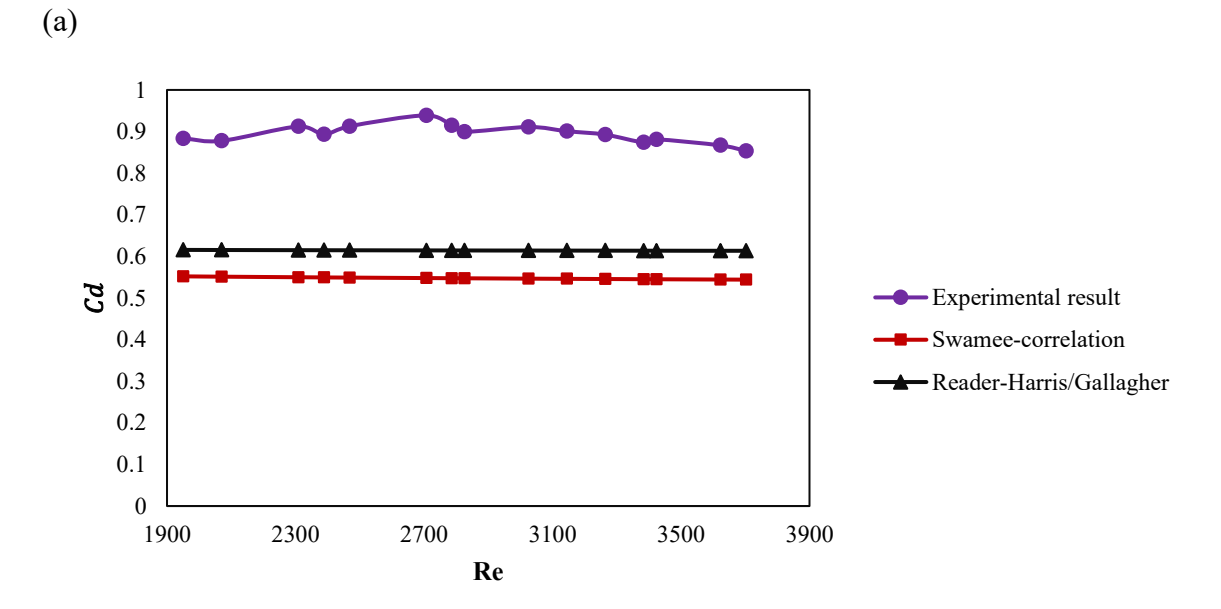
$$C_{d,Exp} = \frac{Q_{act}\sqrt{1 - \beta^4}}{a\sqrt{2gH}}$$

where:

- a is the orifice area
- $\beta$  is the ratio of orifice diameter (d) to pipe diameter (D)
- *H* is the head difference across the orifice plate

The Agreement between the empirical and experimental values would confirm the suitability of the classical correlations for the geometries and flow conditions used in this study, even as Reynolds numbers approach the transitional regime and cavitation begins. In contrast, significant deviations would highlight the limits of these models once vapor formation affects jet contraction and discharge behavior. It is important to note that these empirical formulas were originally developed for non-cavitating conditions; therefore, the comparison also highlights the influence of cavitation and the limitations of existing empirical correlations under the present Reynolds number range, orifice geometry, and cavitating conditions.

Also, given the known relationship between head loss coefficient and discharge coefficient, where  $k = 1 / C_d^2$ , The evolution of  $C_d$  directly reflects changes in energy dissipation. A decline in  $C_d$  indicates rising losses and, when Cv < 1, marks the onset of cavitation-dominated flow behavior. Equivalent plots are reported for each tested orifice diameter in the following figures.



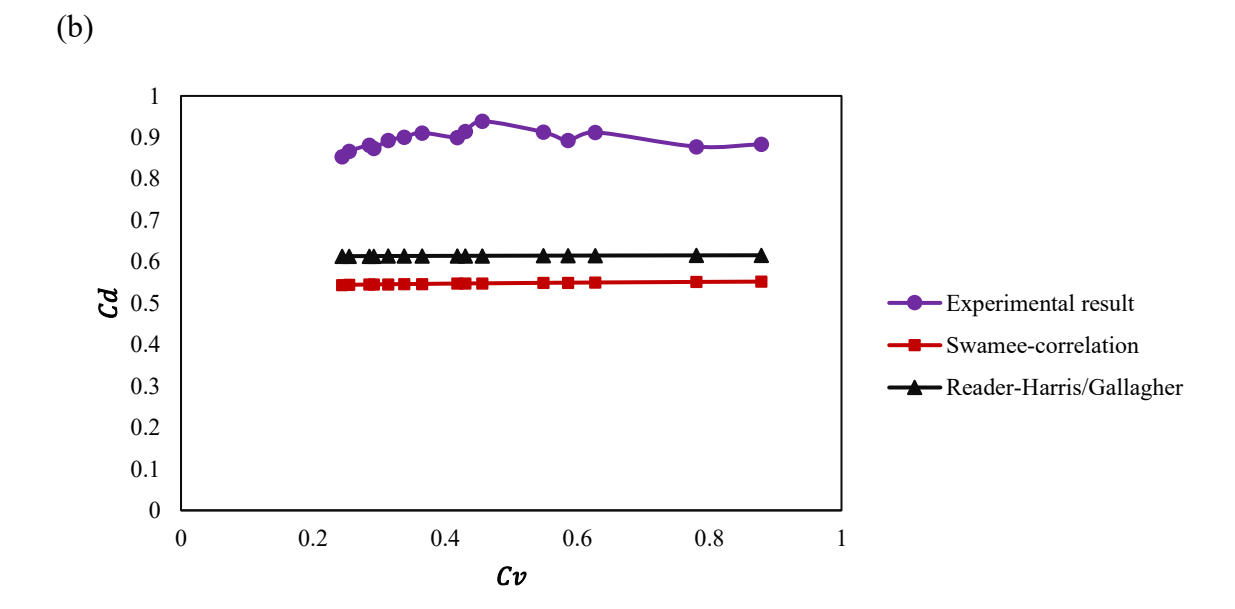
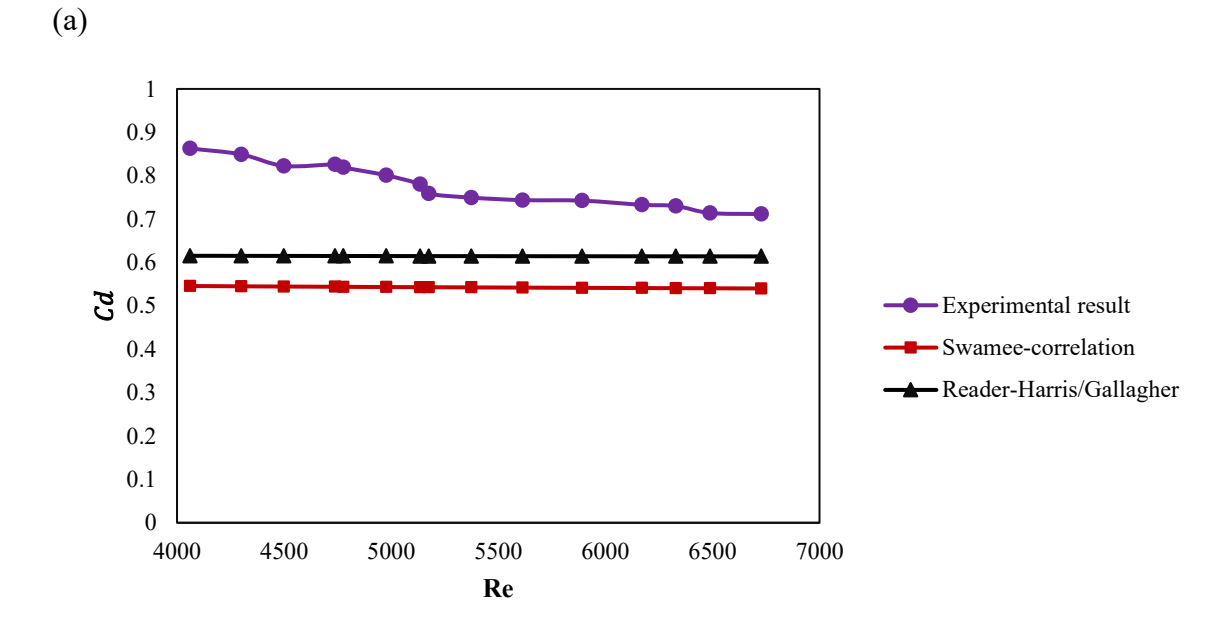


Figure 17 Comparison between experimental and empirical discharge coefficients for the 2 mm orifice:(a) variation of  $\mathcal{C}_d$  with Reynolds number;(b) variation of  $\mathcal{C}_d$  with cavitation number.



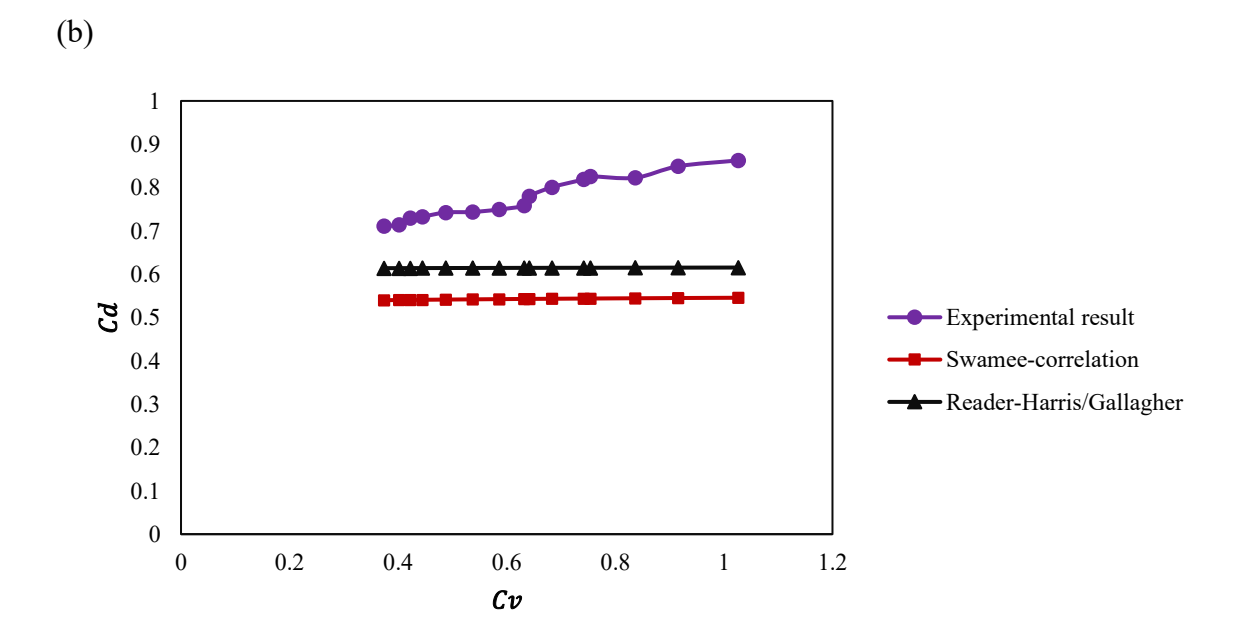
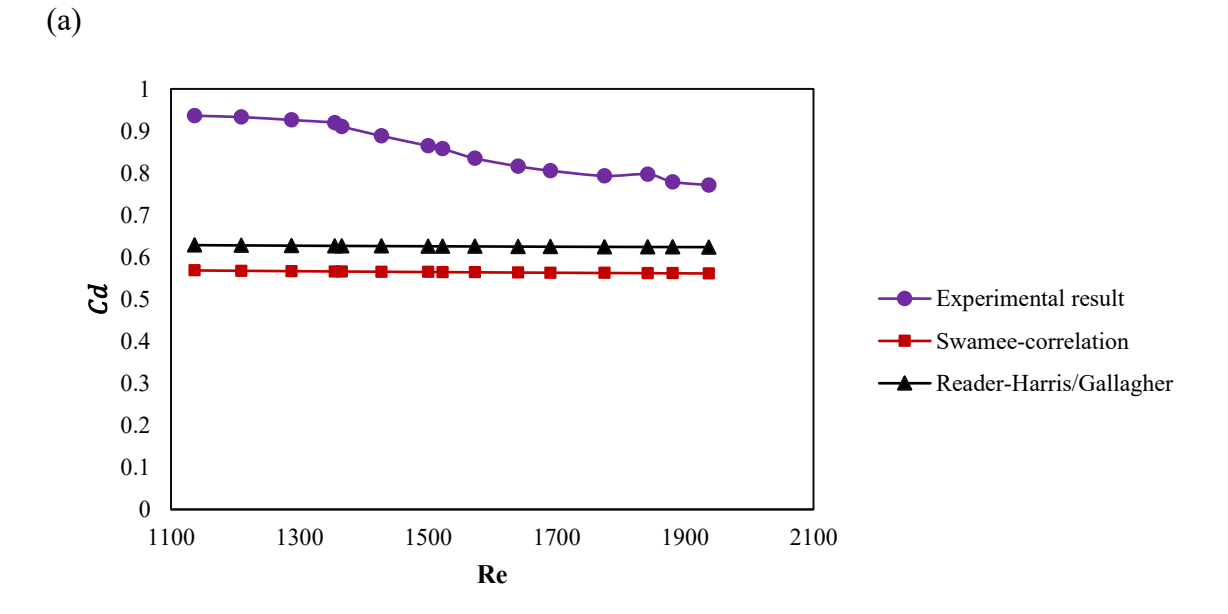


Figure 18 Comparison between experimental and empirical discharge coefficients for the 3 mm orifice:(a) variation of  $C_d$  with Reynolds number;(b) variation of  $C_d$  with cavitation number.



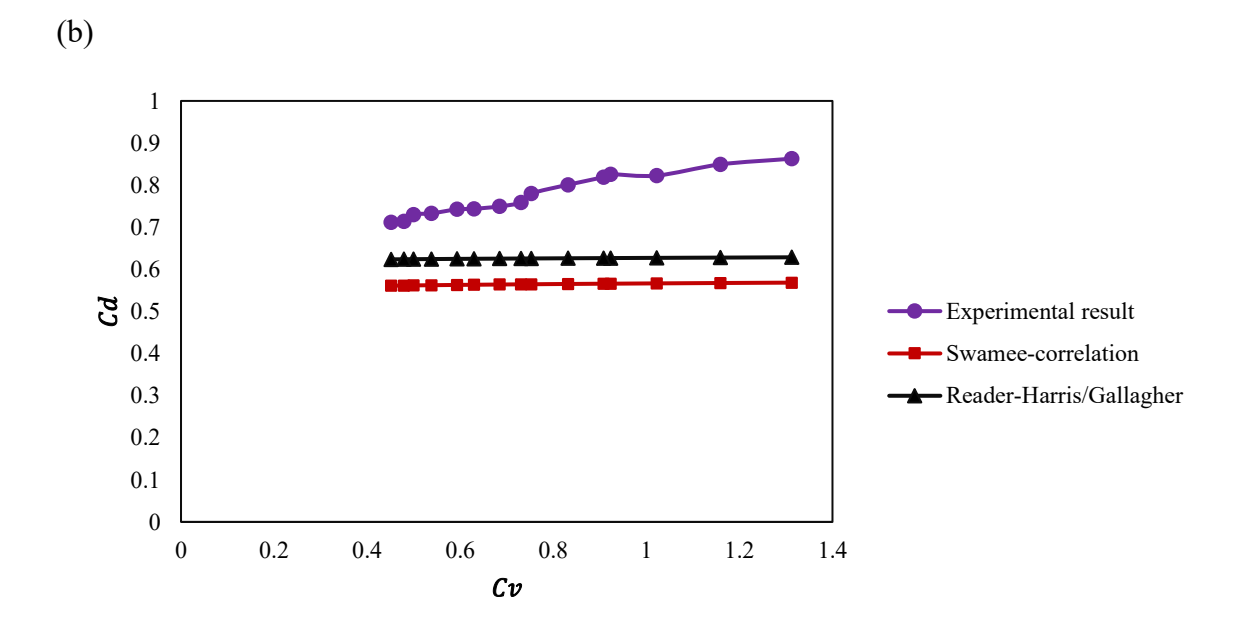
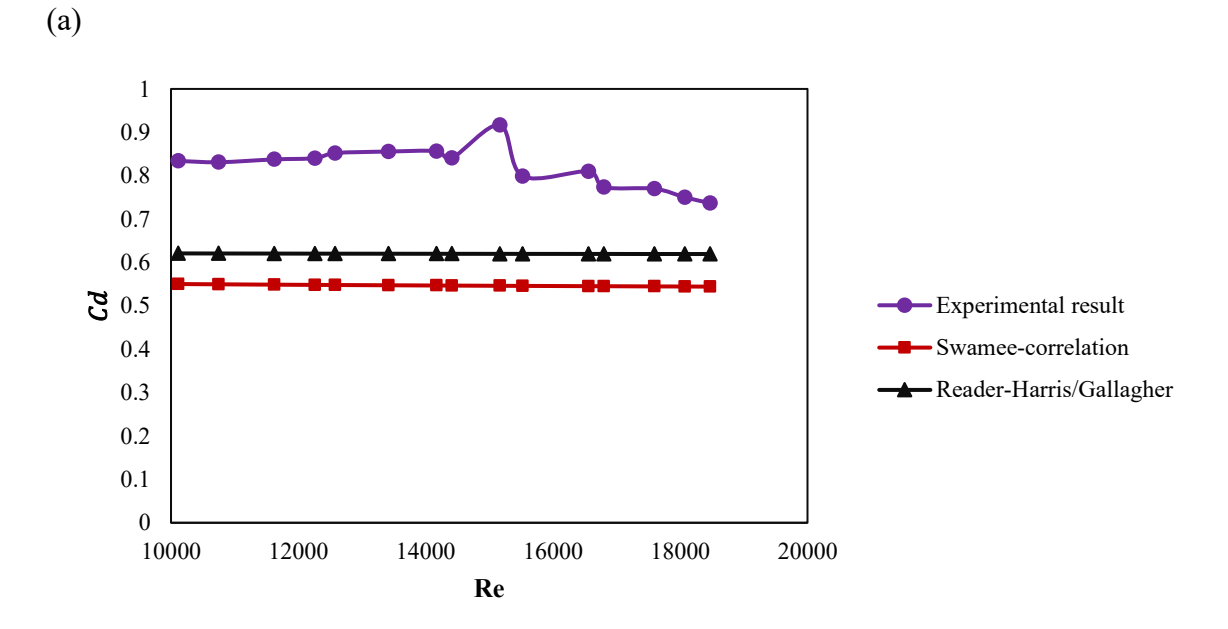


Figure 19 Comparison between experimental and empirical discharge coefficients for the 4.5 mm orifice:(a) variation of  $C_d$  with Reynolds number;(b) variation of  $C_d$  with cavitation number.



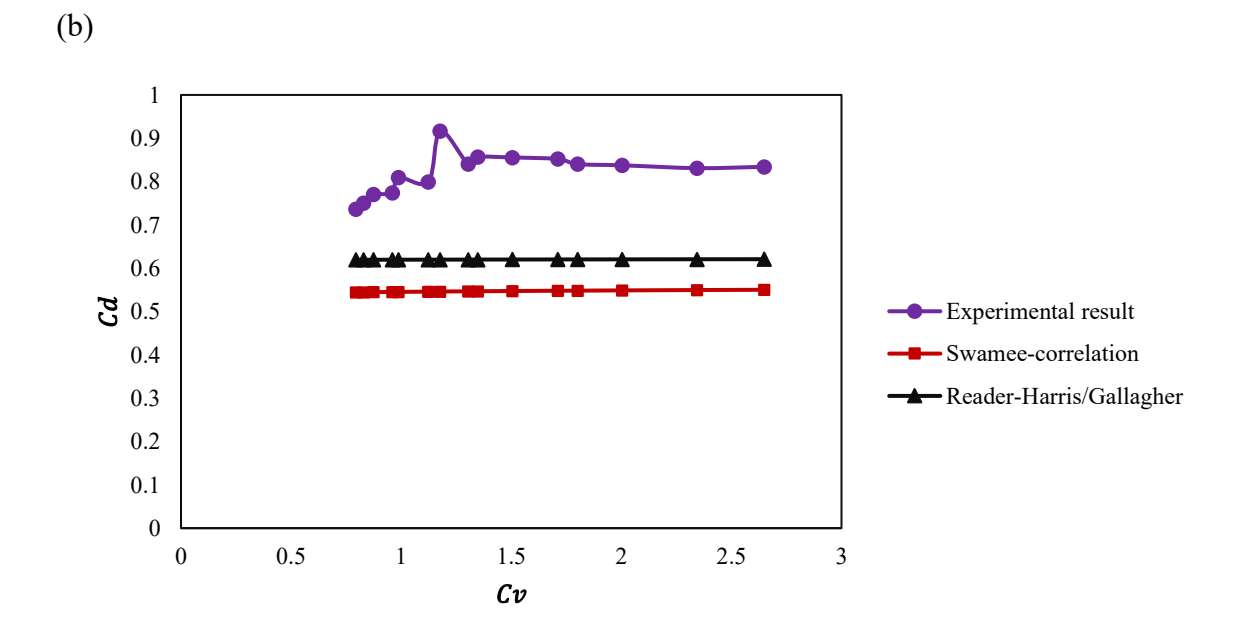


Figure 20 Comparison between experimental and empirical discharge coefficients for the 6 mm orifice:(a) variation of  $C_d$  with Reynolds number;(b) variation of  $C_d$  with cavitation number.

Experimental data show discharge coefficients in the range of  $C_d \approx 0.80$  for every plate, well above the values predicted by correlations of Swamee ( $\approx 0.55$ ) and Reader-Harris/Gallagher ( $\approx 0.61$ ). Across all diameters,  $C_d$  decreases mildly as Re rises; the empirical curves remain virtually flat. The disparity grows with increasing Re, emphasising that the classical correlations lose accuracy once the flow regime begins to approach cavitation. When Cv falls below  $\approx 1$ , the experimental  $C_d$  drops sharply, whereas the empirical lines stay constant. This break-point marks cavitation onset, confirming that vapor formation enlarges the jet contraction and reduces discharge efficiency.

For the smallest orifice diameter, Cv remained below 1 throughout every test, indicating a permanently cavitating jet.  $C_d$  is therefore almost flat with Re, demonstrating that under strong cavitation, the Reynolds number becomes less effective; geometry and vapor content dominate. The hydraulic flip described by Chemloul (2012) is effectively reached from the start, so no sudden  $C_d$  collapse is observed.

For the larger orifices, Cavitation onset is captured within the test window.  $C_d$  stays high and slowly decays while Cv > 1, then falls abruptly once  $Cv \approx 1$  (most pronounced for the 6 mm plate), mirroring Chemloul's sharp-edged results and stabilising in a post-flip plateau.

The systematic over-prediction of losses by Swamee and Reader-Harris/Gallagher confirms their limited validity outside the published Re- $\beta$  envelope and under cavitating conditions.

Since  $k = 1 / C_d^2$ , the observed  $C_d$  patterns translate directly into the head-loss trends. The strong  $C_d$  decline at low Cv corresponds to the rise in k, which is attributed to vapor-bubble growth and collapse.

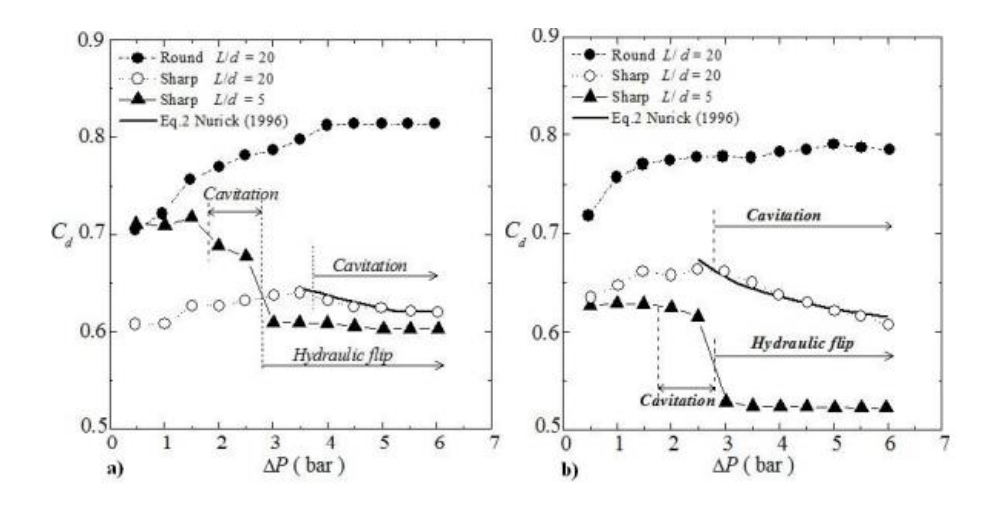


Figure 21 Discharge-coefficient trends for round- and sharp-edged orifices as a function of injection pressure differential  $\Delta P$ , illustrating cavitation onset and the subsequent "hydraulic-flip" plateau; (a) d = 0.5 mm and (b) d = 1 mm. Source: Chemloul et al., 2012

### 4.2 Microalgae-Lysis Assessment under Cavitating Flow

This part evaluates whether the characterised hydrodynamic conditions are sufficient to damage *Galdieria sulphuraria* cell walls. A dilute algal suspension was circulated through the hydraulic loop equipped with the 2 mm orifice plate (the configuration that delivered the lowest cavitation number). Sampling and microscopy were used to track any structural changes in the biomass.

A total of 28 L was prepared by diluting 1 L of 6 g / L culture in 27 L of tap water, giving a bulk concentration of 0.214g / L. The frequency was set to 50 Hz, yielding Q = 0 /  $0.93 \frac{L}{s}$ , and  $Cv \approx 0.24$  (lowest attainable with the present pump/orifice pair). Four exposure levels, 10, 20, 30, and 50 turnovers (all 28 L crossing the plate once) were selected. At each

level, 14 mL was withdrawn directly from the loop.Bright-field images of each sample were recorded at 40× magnification and compared to the untreated suspension.

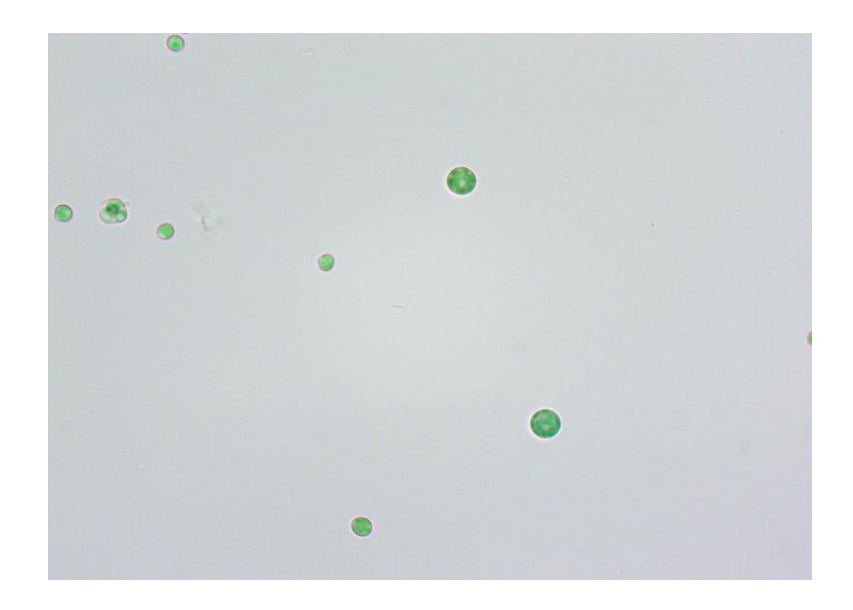
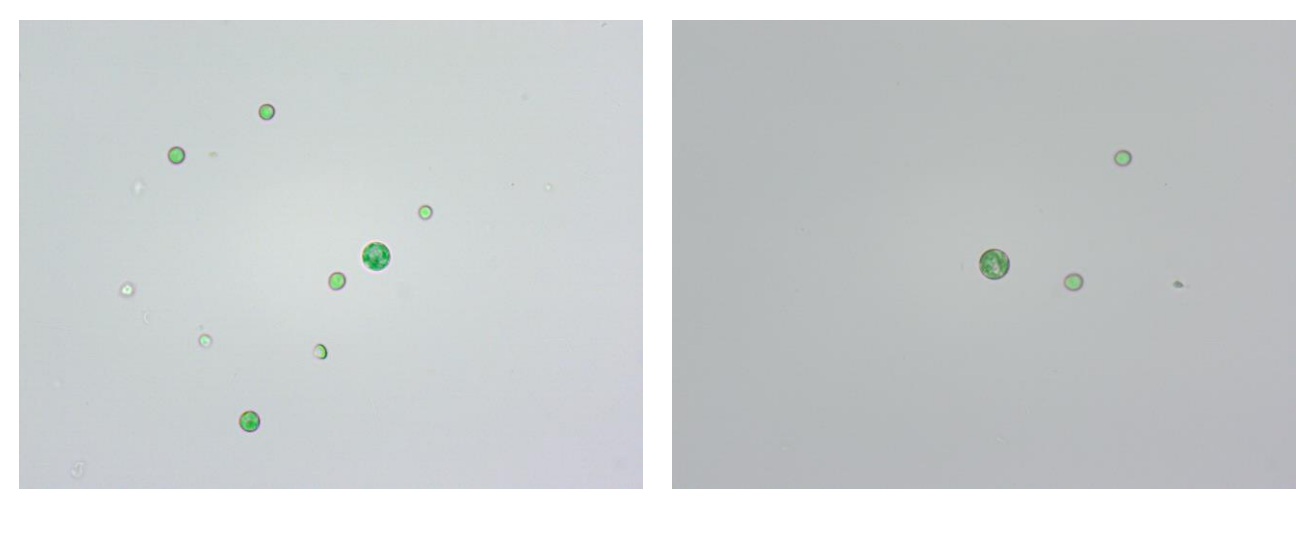


Figure 22 Bright-field micrograph of Galdieria sulphuraria suspension before cavitation treatment (40× magnification).

Representative micrographs are shown in Figure 23. Across all exposure levels, the cells retained their spherical morphology and intact walls; no debris, ghost cells, or obvious ruptures were detected. Visual appearance was indistinguishable from the untreated control (Figure 22).



10 Turnover 20 Turnover

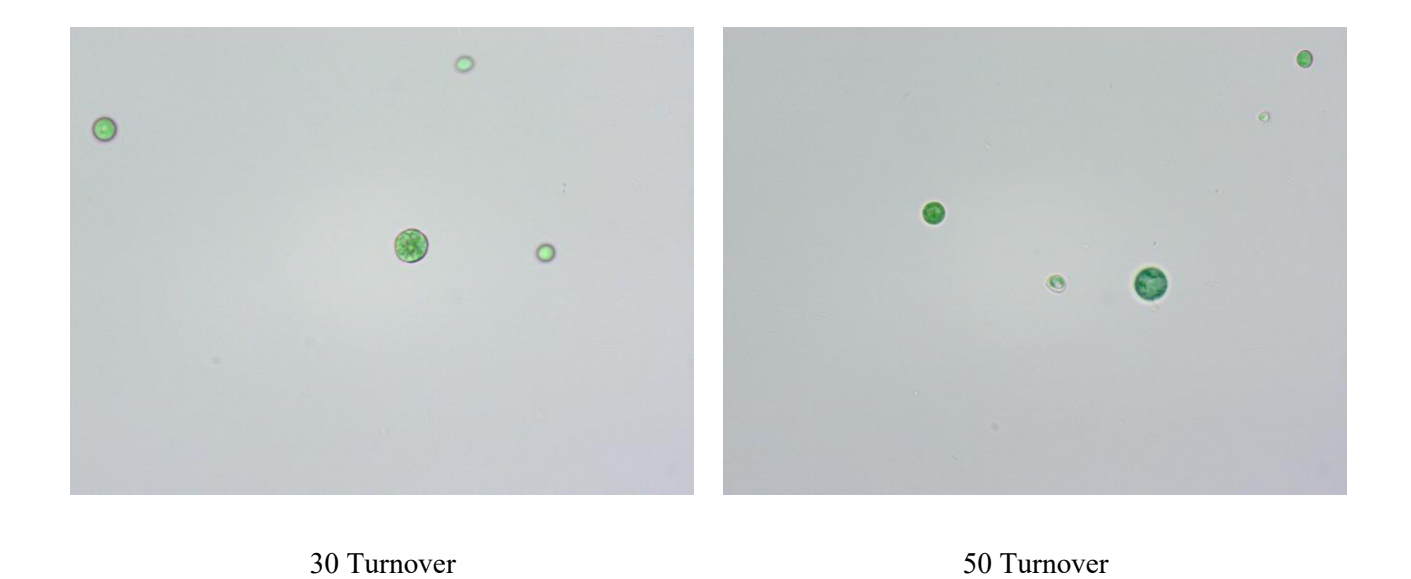


Figure 23 Bright-field microscopic images of Galdieria sulphuraria after 10, 20, 30, and 50 flow turnovers through the hydrodynamic cavitation system (40× magnification)

### 5 Conclusion and Recommendations

This research aimed to explore the potential of an existing hydraulic plant at the Hydraulics and Fluid Mechanics Laboratory of Politecnico di Torino to generate orifice-induced hydrodynamic cavitation capable of breaking microalgal cell walls, with a specific focus on the resilient species *Galdieria sulphuraria*. A comprehensive experimental characterization of the cavitation conditions was carried out using the hydraulic circuit with orifice plates of various diameters (2 mm, 3 mm, 4.5 mm, and 6 mm) to evaluate their influence on cavitation dynamics.

The hydrodynamic characterization revealed critical insights into the influence of orifice diameter on cavitation phenomena. The smallest orifice diameter (2 mm) generated the lowest cavitation number, indicating intense cavitation conditions. However, despite achieving the desired cavitation intensity, the small vapor bubbles generated by this configuration lacked sufficient energy upon collapse to effectively disrupt the robust cell walls of Galdieria sulphuraria. Conversely, larger orifice diameters produced larger vapor bubbles with greater collapse energy but failed to attain sufficiently low cavitation numbers due to limited fluid velocity. This critical trade-off between cavitation number and bubble size is a primary factor influencing the effectiveness of hydrodynamic cavitation in cell disruption applications.

The analysis of the head-loss coefficient k demonstrated a clear dependence on Reynolds number and orifice diameter. Experimental discharge coefficients were evaluated and compared against empirical correlations from literature to identify a suitable predictive model for head-loss behavior. Significant deviations from empirical correlations under cavitating conditions highlighted the limitations of existing theoretical models when applied to cavitating flows. Thus, the variation observed in the discharge coefficient under cavitating conditions directly influenced the calculated head-loss coefficients, underscoring the sensitivity of hydraulic performance to cavitation phenomena and geometric characteristics. Among the tested configurations, the 2 mm orifice consistently

exhibited the lowest head-loss coefficient values, indicating relatively lower energy dissipation compared to larger diameters.

Microscopic examination of algae samples after treatment clearly indicated no significant cell wall rupture or structural damage under tested conditions, affirming the ineffectiveness of the selected orifice configurations for lysing *Galdieria sulphuraria*.

Further design improvements are required to simultaneously achieve lower cavitation numbers and larger bubble sizes. Custom-designed orifice geometries, such as advanced Venturi-type configurations, may yield more favorable cavitation conditions. Implementing pumping solutions capable of higher fluid velocities and more controlled pressure drops is recommended to achieve more intense cavitation regimes suitable for robust cell disruption. The Venturi design developed in this research, presented in Appendix A, shows potential for creating favorable cavitation conditions and warrants further investigation for effective cell disruption.

In conclusion, although hydrodynamic cavitation demonstrates significant potential as a sustainable microalgae pretreatment method, achieving effective cell disruption requires careful balancing of hydrodynamic parameters. Continued research and optimization, informed by detailed hydrodynamic analyses such as those presented here, are crucial to realizing the practical application of this technology in microalgae bioprocessing.

#### References

- Aarthy, A., Kumari, S., Turkar, P., & Subramanian, S. (2018). AN INSIGHT ON ALGAL CELL DISRUPTION FOR BIODIESEL PRODUCTION. *Asian Journal of Pharmaceutical and Clinical Research*, 11(2), 21–26. https://doi.org/10.22159/AJPCR.2018.V11I2.22481
- Adam, N. J., De Cesare, G., & Schleiss, A. J. (2019). Influence of geometrical parameters of chamfered or rounded orifices on head losses. *Journal of Hydraulic Research*, 57(2), 263–271. https://doi.org/10.1080/00221686.2018.1454518
- Arya, S. S., More, P. R., Ladole, M. R., Pegu, K., & Pandit, A. B. (2023b). Non-thermal, energy efficient hydrodynamic cavitation for food processing, process intensification and extraction of natural bioactives: A review. *Ultrasonics Sonochemistry*, *98*, 106504. https://doi.org/10.1016/J.ULTSONCH.2023.106504
- Batista, M. D., Anhê, A. C. B. M., & de Souza Inácio Gonçalves, J. C. (2017). Use of Hydrodynamic Cavitation for Algae Removal: Effect on the Inactivation of Microalgae Belonging to Genus Scenedesmus. Water, Air, and Soil Pollution, 228(11), 1–8. https://doi.org/10.1007/S11270-017-3624-X/FIGURES/5
- Blake, W. K. (2017). Introduction to Bubble Dynamics and Cavitation. *Mechanics of Flow-Induced Sound and Vibration, Volume 1*, 411–467. https://doi.org/10.1016/B978-0-12-809273-6.00006-3
- Brennen, C. E. (2013). *Cavitation and Bubble Dynamics*. https://doi.org/10.1017/CBO9781107338760
- Budiman, A. (2018). Optimum Extraction of Algae-oil from Microalgae using Hydrodynamic Cavitation. *International Journal of Renewable Energy Research*. https://www.academia.edu/105714516/Optimum\_Extraction\_of\_Algae\_oil\_from\_M icroalgae\_using\_Hydrodynamic\_Cavitation

- Carpenter, J., Badve, M., Rajoriya, S., George, S., Saharan, V. K., & Pandit, A. B. (2017). Hydrodynamic cavitation: An emerging technology for the intensification of various chemical and physical processes in a chemical process industry. *Reviews in Chemical Engineering*, 33(5), 433–468. https://doi.org/10.1515/REVCE-2016-0032
- Chai, T., Mo, X., Xu, S., Cheng, H., Long, X., & Zhang, Z. (2025). Removal of Microcystis aeruginosa using hydrodynamic cavitation in a jet pump cavitation reactor: Considering the mechanical and chemical effects. *Journal of Environmental Management*, 390, 126264. https://doi.org/10.1016/J.JENVMAN.2025.126264
- Chemloul, N. S. (2012). Experimental Study of Cavitation and Hydraulic Flip Effects on Liquid Jet Characteristics into Crossflows. *Journal of Applied Fluid Mechanics*, *5*(4), 33–43. https://doi.org/10.36884/JAFM.5.04.19458
- Essien, S., Archibong-Eso, A., & Lao, L. (2019). DISCHARGE COEFFICIENT OF HIGH VISCOSITY LIQUIDS THROUGH NOZZLES. *Experimental Thermal and Fluid Science*, 103, 1–8. https://doi.org/10.1016/j.expthermflusci.2019.01.004
- Franc, J.-P., & Michel, J.-M. (2005). *Fundamentals of Cavitation*. 76. https://doi.org/10.1007/1-4020-2233-6
- Gogate, P. R., & Kabadi, A. M. (2009). A review of applications of cavitation in biochemical engineering/biotechnology. *Biochemical Engineering Journal*, 44(1), 60–72. https://doi.org/10.1016/J.BEJ.2008.10.006
- Gogate, P. R., & Pandit, A. B. (2005). A review and assessment of hydrodynamic cavitation as a technology for the future. *Ultrasonics Sonochemistry*, *12*(1–2), 21–27. https://doi.org/10.1016/J.ULTSONCH.2004.03.007
- Greenly, J. M., & Tester, J. W. (2015). Ultrasonic cavitation for disruption of microalgae.

  \*Bioresource Technology, 184, 276–279.

  https://doi.org/10.1016/J.BIORTECH.2014.11.036

- IDELCHIK, I. E. . (2008). Handbook of hydraulic resistance. https://www.scribd.com/document/511743280/Handbook-of-Hydraulic-Resistanceby-I-E-Idelchik
- ISO 5167-2:2022 Measurement of fluid flow by means of pressure differential devices inserted in circular cross-section conduits running full Part 2: Orifice plates. (n.d.). Retrieved July 7, 2025, from https://www.iso.org/standard/79180.html
- Jianhua, W., Wanzheng, A., & Qi, Z. (2010). Head loss coefficient of orifice plate energy dissipator. *Journal of Hydraulic Research*, 48(4), 526–530. https://doi.org/10.1080/00221686.2010.507347;JOURNAL:JOURNAL:TJHR20;RE QUESTEDJOURNAL:JOURNAL:TJHR20;WGROUP:STRING:PUBLICATION
- Kim, I., Lee, I., Jeon, S. H., Hwang, T., & Han, J. I. (2015). Hydrodynamic cavitation as a novel pretreatment approach for bioethanol production from reed. *Bioresource Technology*, *192*, 335–339. https://doi.org/10.1016/j.biortech.2015.05.038
- Lee, A. K., Lewis, D. M., & Ashman, P. J. (2015). Microalgal cell disruption by hydrodynamic cavitation for the production of biofuels. *Journal of Applied Phycology*, 27(5), 1881–1889. https://doi.org/10.1007/S10811-014-0483-3/TABLES/2
- Maynes, D., Holt, G. J., & Blotter, J. (2013). Cavitation inception and head loss due to liquid flow through perforated plates of varying thickness. *Journal of Fluids Engineering, Transactions of the ASME*, 135(3). https://doi.org/10.1115/1.4023407
- Moholkar, V. S., & Pandit, A. B. (2001). Modeling of hydrodynamic cavitation reactors: a unified approach. *Chemical Engineering Science*, 56(21–22), 6295–6302. https://doi.org/10.1016/S0009-2509(01)00253-6
- Munson, B. Roy., Okiishi, T. H. ., Huebsch, W. W. ., & Rothmayer, A. P. . (2013). Fundamentals of fluid mechanics. 10.

- Phan, T. H., Nguyen, V. T., Duy, T. N., Kim, D. H., & Park, W. G. (2022). Influence of phase-change on the collapse and rebound stages of a single spark-generated cavitation bubble. *International Journal of Heat and Mass Transfer*, 184, 122270. https://doi.org/10.1016/J.IJHEATMASSTRANSFER.2021.122270
- Rahman, M. M., Hosano, N., & Hosano, H. (2022). Recovering Microalgal Bioresources: A Review of Cell Disruption Methods and Extraction Technologies. *Molecules 2022, Vol. 27, Page 2786, 27*(9), 2786. https://doi.org/10.3390/MOLECULES27092786
- Retta, B., Iovinella, M., & Ciniglia, C. (2024). Significance and Applications of the Thermo-Acidophilic Microalga Galdieria sulphuraria (Cyanidiophytina, Rhodophyta). Plants 2024. Vol. 13. 1786, *13*(13), 1786. Page https://doi.org/10.3390/PLANTS13131786
- Sarkar, P., Ghigliotti, G., Franc, J. P., & Fivel, M. (2021). Mechanism of material deformation during cavitation bubble collapse. *Journal of Fluids and Structures*, *105*, 103327. https://doi.org/10.1016/J.JFLUIDSTRUCTS.2021.103327
- Shivakumar, S., Serlini, N., Esteves, S. M., Miros, S., & Halim, R. (2024). Cell Walls of Lipid-Rich Microalgae: A Comprehensive Review on Characterisation, Ultrastructure, and Enzymatic Disruption. *Fermentation 2024, Vol. 10, Page 608*, 10(12), 608. https://doi.org/10.3390/FERMENTATION10120608
- Sousa, V., Pereira, R. N., Vicente, A. A., Dias, O., & Geada, P. (2023). Microalgae biomass as an alternative source of biocompounds: New insights and future perspectives of extraction methodologies. *Food Research International*, *173*, 113282. https://doi.org/10.1016/J.FOODRES.2023.113282
- Sumeru, H. A., Nurrusyda, F. S., Rachmadona, N., Khoo, K. S., & Show, P. L. (2025b).
  Intensified cavitation process for the pretreatment of microalgae: a mini review.
  Current Opinion in Chemical Engineering, 48, 101142.
  https://doi.org/10.1016/J.COCHE.2025.101142

- Sydney, T., Marshall-Thompson, J. A., Kapoore, R. V., Vaidyanathan, S., Pandhal, J., & Fairclough, J. P. A. (2018). The Effect of High-Intensity Ultraviolet Light to Elicit Microalgal Cell Lysis and Enhance Lipid Extraction. *Metabolites 2018, Vol. 8, Page 65*, 8(4), 65. https://doi.org/10.3390/METABO8040065
- Waghmare, A., Nagula, K., Pandit, A., & Arya, S. (2019). Hydrodynamic cavitation for energy efficient and scalable process of microalgae cell disruption. *Algal Research*, 40, 101496. https://doi.org/10.1016/J.ALGAL.2019.101496
- Wu, D., Burton, R., & Schoenau, G. (2002). An empirical discharge coefficient model for orifice flow. *International Journal of Fluid Power*, *3*(3), 13–19. https://doi.org/10.1080/14399776.2002.10781143;CTYPE:STRING:JOURNAL
- Zheng, H., Zheng, Y., & Zhu, J. (2022). Recent Developments in Hydrodynamic Cavitation Reactors: Cavitation Mechanism, Reactor Design, and Applications. *Engineering*, 19, 180–198. https://doi.org/10.1016/J.ENG.2022.04.027
  - Save, S. S., Pandit, A. B., & Joshi, J. B. (1994). Microbial cell disruption: role of cavitation. The Chemical Engineering Journal and the Biochemical Engineering Journal, 55(3), B67–B72. https://doi.org/10.1016/0923-0467(94)06062-2
  - Setyawan, M., Mulyono, P., Sutijan, Pradana, Y. S., Prasakti, L., & Budiman, A. (2020). Effect of devices and driving pressures on energy requirements and mass transfer coefficient on microalgae lipid extraction assisted by hydrodynamic cavitation. *International Journal of Renewable Energy Development*, 9(3), 467–473. https://doi.org/10.14710/IJRED.2020.26773

# Appendix

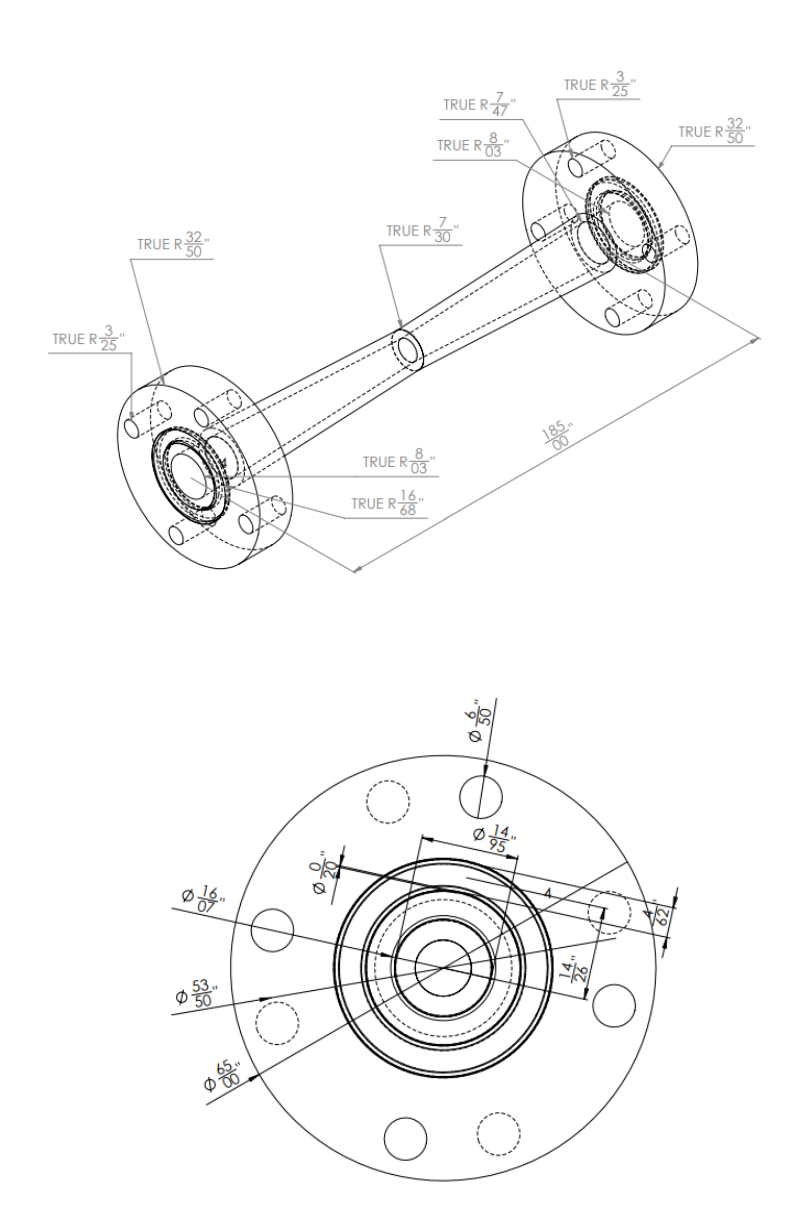


Figure 24 Appendix A .Suggested Venturi Design with Flange Connections – Dimensional and Assembly Drawings